K. Pielichowski, K. Pielichowska. Polymer nanocomposites, in: S. Vyazovkin, N. Koga, C. Schick (Eds.) Handbook of Thermal Analysis and Calorimetry, Elsevier Science B.V. 2018, pp. 431-485.

Chapter 11

Polymer Nanocomposites

Krzysztof Pielichowski* and **Kinga Pielichowska†**
*Cracow University of Technology, Krakow, Poland
†AGH University of Science and Technology, Krakow, Poland

ABBREVIATIONS

AFM	atomic force microscopy
BMA	butyl methacrylate
CNCs	cellulose nanocrystals
CNFs	cellulose nanofibrils
DETA	dielectric thermal analysis
DFSC	differential fast scanning calorimetry
DMA	dynamic mechanical analysis
DRS	dielectric spectroscopy
DSC	differential scanning calorimetry
EP	epoxy resin
FTIR	Fourier transformed infrared spectroscopy
GO	graphene oxide
HAp	hydroxyapatite
HSC	hybrid shish-calabash
HSK	hybrid shish-kebab
ID	interparticle distance
LTA	localized thermal analysis
MAF	mobile amorphous fraction
MMT	montmorillonite
MS	mass spectrometry
MWCNTs	multiwalled carbon nanotubes
NCG	nanoporous cellulose gels
NDs	nanodiamonds
NPs	nanoparticles
PA	polyamide
PBSu	poly(butylene succinate)
PE	polyethylene
PEX	cross-linked polyethylene

Handbook of Thermal Analysis and Calorimetry, Vol. 6. https://doi.org/10.1016/B978-0-444-64062-8.00003-6

PEG	poly(ethylene glycol)
PEMA	poly(ethyl methacrylate)
PEO	poly(ethylene oxide)
PET	poly(ethylene terephthalate)
PLA	poly(lactic acid)
PLS	polymer/layered silicate
PMMA	poly(methyl methacrylate)
PNCs	polymer nanocomposites
POM	polyoxymethylene
POSS	polyhedral oligomeric silsesquioxanes
PS	polystyrene
PU	polyurethane
RAF	rigid amorphous fraction
SEM	scanning electron microscopy
SWNTs	single-wall carbon nanotubes
TEM	transmission electron microscopy
TGA	thermogravimetric analysis
TMA	thermomechanical analysis
TMDSC	temperature modulated DSC

11.1 INTRODUCTION

In the field of nanotechnology, one of the most popular areas for current research and development are polymer nanocomposites (PNCs), and the investigation field covers a broad range of topics. This would include nanoelectronics, polymeric bionanomaterials, reinforced PNCs, nanocomposite-based drug delivery systems, etc.

According to theoretical assumptions, idea of PNCs is based on the concept of creating a very large interface between the nanosized heterogeneities and macromolecules of neat polymer. The large interface between nanoparticles and macromolecules are supposed to result in unusual properties relative to conventional microfilled polymer composites. In nanocomposites, large reinforcement and enhancing of other properties like decreased flammability and increased conductivity are often obtained at low concentration of nanofillers. However, those effects strongly depend on the homogeneous distribution of the nanoadditive in the polymer matrix that is hard to achieve.

For example, in case of polymer/montmorillonite (MMT) nanocomposites the limited degree of exfoliation, and in consequence the number of separated MMT platelets produced, is a major problem in composites containing platelike reinforcement that leads to the formation of a number of structures with different degree of exfoliation and intercalation [1–3]. In case of PNCs containing fibers, tubes, or spherical nanoparticles it is difficult to avoid aggregation mainly due to high viscosity of polymer melt. To define and explain the

synergistic advantage of nanoscale additives on PNCs properties, often called "nano-effect" or their absence in relation to micro- or larger-scale additives, different analytical methods are necessary. To understand the property changes of polymer matrix, what is crucial is recognizing the behavior of macromolecules in the presence of nanoparticles or nanofibers that is important to optimization of the nanocomposite properties and to expanding the limits in property enhancement. Nanosized additives can change mechanical properties, barrier properties, flame resistance, electrical and optical properties, and thermal properties [4]. To follow the changes in properties appropriate methods should be used, for example, thermal analysis methods. Hence, in this chapter application of different thermal analysis methods, such as differential scanning calorimetry (DSC) and modulated temperature DSC (TMDSC), thermogravimetric analysis (TGA) and TG hyphenated with Fourier transformed infrared spectroscopy (FTIR) and MS, thermomechanical analysis (TMA), dynamic mechanical analysis (DMA), localized thermal analysis (LTA), and dielectric thermal analysis (DETA), in the PNCs field will be described. It will be shown how thermal analysis methods can help to explain "nano-effects" observed in polymeric nanocomposites and how they are applied in the determination of phase transitions and degradation processes of nanostructured polymeric materials.

11.2 PNCs

The size of nanomaterials are within the range of 1–100 nm in at least one dimension and exhibit different physical, chemical, and biological properties and functions than the same material in microscale [5–7]. Consequently, PNCs can be defined as polymers containing fillers of different shape with one dimension smaller than 100 nm. Moreover, in contrast to conventional polymer composites with high loadings (even up to 60 vol%) of microsized filler, PNCs contain usually low loadings (less than 5 vol%) of nanofillers [8]. Nanofillers can be classified by their geometries as particle, layered, and fibrous materials [7,8]. Carbon black, silica nanoparticle, polyhedral oligomeric silsesquioxanes (POSS) can be classified as nanoparticles, while cellulose nanofibers and carbon nanotubes are examples of fibrous materials [8]. Nanofillers with nanometer thickness, high aspect ratio (30–1000), and plate-like structure are classified as layered nanomaterials, and the examples are layered silicates, for example, MMT, or graphite [9].

11.3 NANO-EFFECTS IN PNCs

Nanoparticles added to polymer matrix can tune thermal, thermomechanical, electric, optical, and magnetic properties of matrix materials. Depending on the shape, size, amount, chemical structure, and the polymer radius of gyration, the addition of nanoparticles can enhance or slow down polymer chain

dynamics [10]. It was described that PNCs containing nanoparticles smaller than the random coil size of their host polymer chains exhibited unique properties, such as lower viscosity and glass-transition temperature in comparison to the unmodified polymer melt due to fast diffusion of the nanostructures in the host polymer, which facilitates polymer chain relaxation by constraint release and other processes [11].

11.3.1 Confinement Effects

Currently, in the era of dynamic development of nanotechnology, there is considerable interest in the determination of properties of polymers confined in nanometer scale spaces. Numerous efforts have been taken to better understand confinement effects on the polymer chains during thermal transitions that occur in the presence of particles with reduced dimensionality. That is crucial for the thermal behavior and mechanical properties of thin polymer films, nanocomposites, porous materials, and nanofibers [12].

The dynamics of polymer chains under confinement is in general very different from that in the bulk, especially when the confining dimensions are similar or smaller than the polymer coil size [13]. There are two kinds of nanoconfinement effect in PNCs: first, polymer chains are effectively pinned at the surfaces of nanoparticles (NPs) due to the interactions between nanoparticles and the chain; second, chain mobility close to the nanoparticles is strongly hindered thus creating an interfacial phase. It was reported that the interfacial polymer can be a significant volume fraction of nanocomposites and exhibits different crystallization behaviors from bulk phase [14]. Also, Monte Carlo simulations of PNCs show that even above the glass-transition temperature, nanoparticles induce the formation of a solid-like, glassy layer characterized by large elastic moduli. The existence of glassy layer can explain the experimentally observed increase of the storage modulus in nanocomposites. Below the glass temperature, the presence of the nanoparticles can reduce the degree of mechanical in homogeneity, so that the nanocomposite glasses are not only stronger, but also more resistant to failure [15]. Enhanced properties of PNCs is closely related to the modified polymer dynamics in the interfacial phase.

The second type of nanoconfinement is connected to spatial constraints of polymer chains confined in the restricted space between NPs. With an increase of NP loading, the distance between neighboring NPs become smaller, or NP aggregates in consequence will lead to the growing steric obstacles to the polymer crystallization [16]. The influence of geometric confinement on the crystallization behaviors of nanocomposites strongly depends on the distribution of nanoparticles and polymer matrix. A good dispersion is required since the nanoparticle aggregation will result in an effective larger interparticle distance (ID) and no significant nanoconfinement effects will be observed on the chain mobility of polymers [16,17].

Composto group investigated macromolecular diffusion in a PNC [polystyrene (PS) or poly(methyl methacrylate) (PMMA) with nanosilica] [18,19]. The confinement parameter was defined as the ratio of the ID relative to the probe size, $2R_g$, where R_g is the radius of gyration of the polymer tracer chain. ID/$2R_g$ represents the melt region available for polymer chains to diffuse between a fixed array of randomly placed nanoparticles. Under the assumption that NP are well dispersed and randomly distributed in the polymer matrix, ID was calculated as

$$\mathrm{ID} = d_n \left[\left(\frac{2}{\phi_{NP}\pi} \right)^{1/3} e^{\ln \sigma^2} - 1 \right] \tag{11.1}$$

As it can be seen, ID depends on nanoparticle size (d_n), nanoparticle volume fraction (ϕ_{NP}), and nanoparticle size dispersity (σ). The probe size is described by the R_g of polymer assuming that chains obey Gaussian statistics, and given by [20]

$$R_g = \frac{a\sqrt{N}}{\sqrt{6}} = \frac{a\sqrt{M_w/M_0}}{\sqrt{6}} \tag{11.2}$$

where a is the monomer length, N is the degree of polymerization, M_w is the weight-averaged molecular weight, and M_0 is the molar mass of a monomer unit.

It has been observed that for the confinement parameter greater than 1, the diffusion process of PMMA between the immobile nanosilica particles is reduced. For the confinement parameter lower than 1, the PMMA chain size is larger than the average space between particles. Polymer chain then search for a void between particles or its configurational entropy gets lower by squeezing between closely spaced particles. The competition between the former case, corresponding to a limited number of broad pathways, and the latter case of a greater number of narrow pathways, governs the diffusion rate [17].

11.3.2 Entanglement Effects

Dynamics of the interphase region between matrix and polymers bound on nanoparticles is crucial to understand the mechanical and rheological properties of PNCs. The dynamics of long polymer chains is controlled by entanglements that are topological constraints exerted by the neighboring chains. Entanglements can substantially change polymer viscosity, dynamics, mechanical, and tribological properties [21–23]. Generally, there are two theoretical treatments of the dynamical slowing down beyond the entanglement. In the first one based on the Rouse theory [24], collective corrections introduced to the monomer mobility lead both to slowing down and to local anisotropy in polymer. In the second approach, the entanglements are treated phenomenologically, but as serious topological constraints with the most successful tube model. In the tube model, many-body problem was replaced with a tractable single-body

problem. The "single body" is then single polymer chain, and the effective field becomes a tube-like region of constraint along the contour of the chain. In this model, the tube represents the sum of all topological noncrossing constraints active with neighboring chains [22]. The radius of the tube is of the order of the end-to-end length of a chain of molar mass. As a result, only chains with higher molar mass than M_e are strongly affected by the topological constraints. The tube model was introduced in the late 1960s by Edwards [25] for the trapped entanglements in a rubber network, while the consequences of the tube model idea were first studied by de Gennes [26]. Later on, Edwards and Doi developed the tube concept into a theory of entangled melt dynamics and rheology for monodisperse, linear chains [27–30]. The effect of entanglements on the dynamics of filled polymer is described by using the generalized Rouse model (GRM), where the interaction of the representative polymer chain with its neighbors is purely frictional, similar to the original Rouse model [31]. Sarvestani and Picu [32] proposed a frictional molecular model for the viscoelasticity of entangled PNCs. They considered a system of linear monodisperse amorphous homopolymers and a random distribution of nonaggregated rigid spherical nanoparticles uniformly distributed in 3D.

It was assumed that the dispersed nanoparticles are sufficiently small, so that even at low volume fractions the average particle wall-to-wall distance is in the order of the size of the average polymer coil. As a consequence, any polymer chain may simultaneously attach to one or more nanoparticles while each adsorbed polymer chain section includes a succession of disperse loops and train segments. However, there is a large number of disperse dangling tails in the matrix—segments connected at one end to the filler and having the other end free. This model focuses on capturing two major effects: entanglements and the process of attachment/detachment of chains from nanoparticles—these effects are supposed to play a key role in the rheology of PNCs. In the proposed approach, the polymer chain dynamics is modeled using classical concepts of polymer physics: the entanglements are modeled using the GRM, while the stick-slip process of the chain-filler interaction is modeled in a homogenized way through an additional friction force [32].

There was an effect of NPs on the Rouse time for entanglement segments—even at low particle concentrations, polymer-functionalized NPs provide additional tube-like constraints on chain relaxation that leads to an earlier onset of reptation relaxation (Fig. 11.1).

It has been postulated that on long timescales, nanoparticle motions appear to degrade the tube surroundings of their host chains, which accelerates tube escape by a process analogous to constraint release in mixtures of entangled polymers with widely differing molecular weights. In well-entangled materials these processes lead to an apparent lowering of the viscosity of the host polymer at low NP concentrations [33].

For the PNCs with inorganic nanoparticles interacting weakly with the polymer matrix, confinement effects and chain disentanglements in the presence of

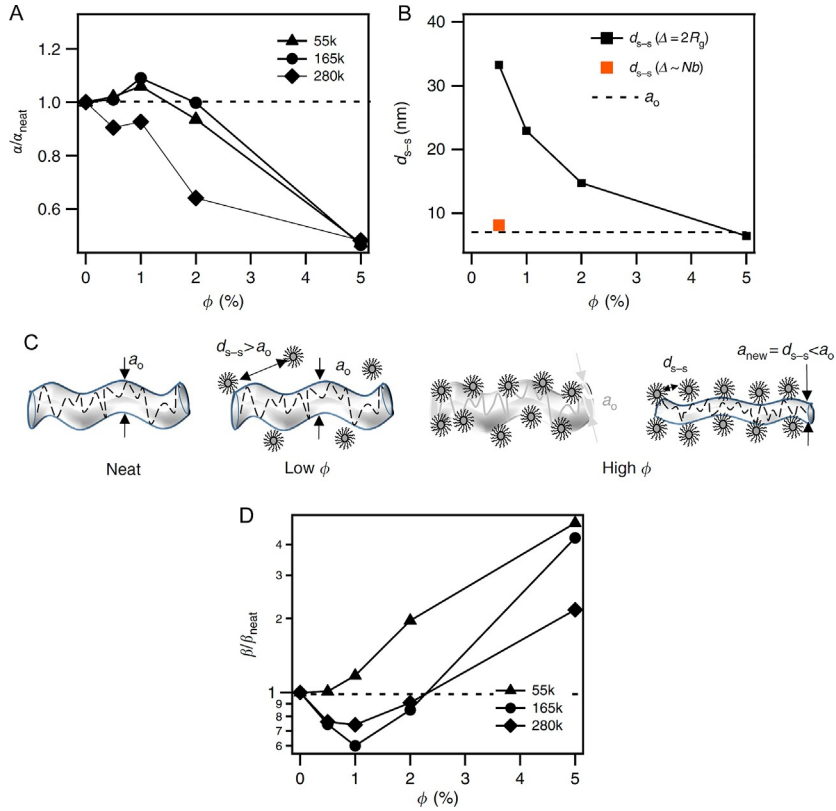

FIG. 11.1 Effect of NPs on entanglement tube diameter and effective number of entanglements of host polymer chains. (A) The effect of NP volume fraction on $\alpha \equiv (\tau_e/\tau_0)^{1/4} = a_e/b$ for PNCs with respect to the particle-free melt. (B) Surface-to-surface distance ($d_{s-s} = d_{p-p} - (2\Delta + D)$), for $\Delta = 2R_g$ and $\Delta \sim N_b$, as a function of particle content. The *dashed horizontal line* corresponds to the tube diameter (a_o) of the host polymer. (C) Schematic of the mechanism through which hairy NPs exert entanglement-like constraints on polymer chains in a PNC. (D) $\beta \equiv (\tau_t/\tau_e)^{1/3} = 3^{1/3}Z$ vs NP volume fraction for PNCs with respect to particle-free polymer melts. *Reprinted from R. Mangal, S. Srivastava, L.A. Archer, Phase stability and dynamics of entangled polymer-nanoparticle composites, Nat. Commun. 6 (2015) 7198 with permission from Nature Publishing Group.*

well-dispersed interfaces affect viscosity of the composite systems; the decrease and recovery of the entanglements by vitrification and softening of the bound polymer aligns with the softening-stiffening transition of bulk composites [34].

Karatrantos et al. [23] postulated that for formation of polymer nanoparticles entanglements, the polymers need to be substantially larger than the nanoparticles in order to wrap around them, and in that case the nanoparticles act as topological constraints. Moreover, the total entanglement length was not affected by the interaction between polymers and nanoparticles, provided fine nanoparticle dispersion was achieved.

11.3.3 The Influence of Nanoparticles on Glass Transition

The influence of confinement effect on T_g for polymers has been investigated mostly for thin films in the case of one-dimensional confinement. In the mid-1990s, Keddie et al. [35,36] first published results of systematic study on the T_g of polymer films supported on solid substrates as a function of thickness. They found that T_g of PMMA on a gold surface decreases with decreasing film thickness and suggested that at the surface of PMMA, similar to that of PS, there exists a liquid-like layer whose size diverges as the T_g is approached from below. Moreover, it was also found that the T_g of PMMA on the surface of the native oxide of silicon increases slightly with decreasing film thickness probably due to the restriction of mobility of the polymer chains along the interface, caused by hydrogen bonding between PMMA and surface hydroxy groups [36].

However, the polymer chain conformations between nanoparticles may be different from that of thin films. Priestley et al. [37] speculated that nanoparticles suspended in solution may be annealed above T_g for prolonged periods of time for equilibration and NPs could represent a stress-free state of confinement. Additionally, the surface area to volume ratio is much greater for nanoparticles than for thin films.

Crucial for determining the sign and magnitude of the changes in T_g due to geometrical confinement are interactions between NPs and polymer matrix. For example, strong, favorable interactions can increase T_g, while weak or unfavorable interactions can decrease T_g. Starr et al. [38] simulated PNCs over a broad range of polymer matrix-NP interaction strengths. They postulated that with the polymer—polymer interaction getting stronger, a distinct relaxation—slower than the main α-relaxation—arise from an adsorbed macromolecular layer near the nanoparticle surface, which covers it—as a result the dynamics of the polymer matrix is largely unaffected (Fig. 11.2).

The results obtained show that it is possible to explicitly define a distinct fraction of bound polymer with specified relaxation time.

However, Kumar et al. [39] postulated that a simple two-layer model containing regions of modified mobility in the vicinity of the particle surfaces, cannot sufficiently explain the experimental results; interaction of the interphase regions surrounding different particles occurs at the glass transition.

11.3.4 The Influence of Nanoparticles on Polymer Melting and Crystallization

The typical size of polymer lamella is ca. 10 nm thick and a few nanometers to a few micrometers wide. The size of nanoparticles similar to the size (thickness) of polymer lamella suggest that these two seemingly different objects ensures an interesting effect between the polymer single crystals and nanoparticles [40]. At low loadings, the nanoparticles can act as nucleating agent, thus favoring the crystallization process, whereas they may exert confinement on

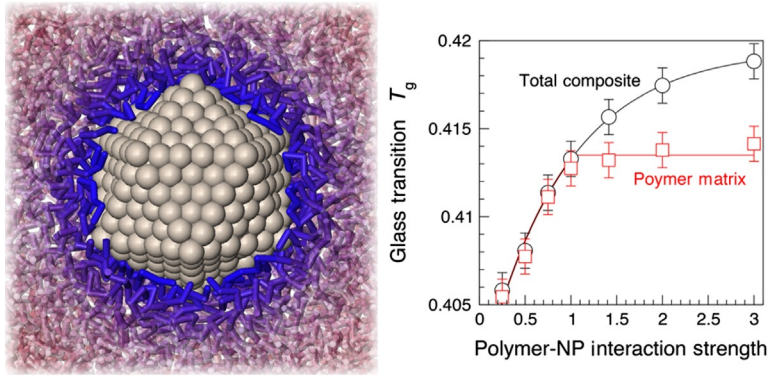

FIG. 11.2 "Bound" polymer layer "cloaks" the NP surface and the influence of polymer-NP interaction strength on glass transition. *Reprinted from F.W. Starr, et al., Bound layers "cloak" nanoparticles in strongly interacting polymer nanocomposites, ACS Nano 10(12) (2016) 10960–10965 with permission from American Chemical Society.*

crystallization at high content [41,42]. In case of filled polymer (nano)composites interfacial crystallization is through the enhanced interaction between polymer and filler caused by the crystallization of polymer on the filler surface. Owing to interfacial crystallization, the kebab/calabash was found in some unique hybrid crystalline structures, including hybrid shish-kebab (HSK) and hybrid shish-calabash (HSC) structures, in which the filler served as the shish and crystalline polymer. It seems that the manipulation of the interfacial crystallization architecture offers high potential to achieve strong polymer/filler interaction.

Nanoparticles can act as nuclei and induce the polymer lamellae growth on the filler surface. New polymer/particle crystalline superstructures are generally denoted as "hybrid crystalline structure" or "hybrid crystal," in contrast to conventional supermolecular crystalline structures such as spherulites, hedrites, or shish-kebab structures (Fig. 11.3).

In PNCs an increase in crystallization rate and crystallization temperature, measured DSC method, as well as a decrease in crystal size were generally observed [41,43].

For nanocomposites with spherical nanoparticles, the hybrid spherulites with smaller size than spherulites of bulk polymer were observed due to the nucleation effect of spherical particles [41].

In PNCs with layered fillers, polymer lamellae decorate the surface of the filler. Nucleation ability of nanofillers depends on surface quality and chemistry as described by Yang et al. [44] who investigated crystallization of isotactic polypropylene (iPP) on the surface of graphene oxide (GO) and reduced GO. Compared to pristine GO, reduced GO displayed superior heterogeneous nucleation effect on iPP crystallization, the lower value of the nucleation

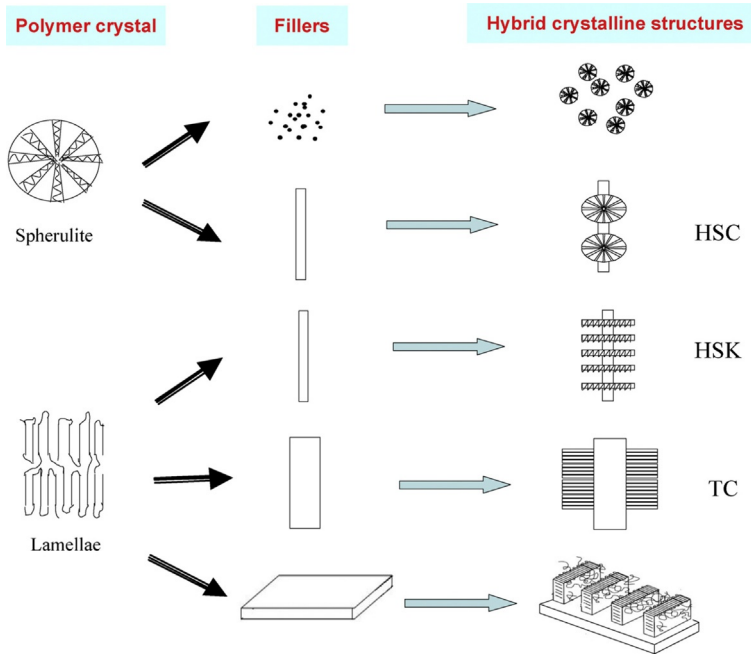

FIG. 11.3 Schematic representation of various hybrid crystalline structures observed in polymer composites and nanocomposites. *Reprinted from N. Ning, et al., Realizing the enhancement of interfacial interaction in semicrystalline polymer/filler composites via interfacial crystallization, Prog. Polym. Sci. 37(10) (2012) 1425–1455 with permission from Elsevier.*

activity and faster overall crystallization rate that suggest mechanism of surface-induced conformational ordering. The removal of functional group from the basal plane of GO was conductive for the molecular formation, activating the conformational ordering and curtailing induction period, but parallel the recovery of sp^2 hybridization of carbon atoms in graphene sheets, which provided extra nucleation sites for the epitaxial growth of iPP lamellar crystals. Authors postulated that the structural integrity of nanolayer played a crucial role in determining the nucleation ability of reduced GO.

In the case of polymer with nanofibrous-filler composites, the transcrystallinity (TC), HSK, or HSC polycrystalline structures were observed [43,45].

TC structure is formed when (nano)fibrous filler initiates a high density of active nuclei on its surface, which hinder the free radial growth of spherulites and therefore force the lamellae to grow in one direction [43,46], as shown in Fig. 11.4.

During isothermal crystallization of poly(lactic acid) (PLA)/poly(ethylene glycol) (PEG) system in the presence of PLA nanofiber at 140°C it can be seen that a large number of primary nuclei regularly align at fiber surfaces, and evoke a rapid crystal growth by involving adjacent PLA chains that fold

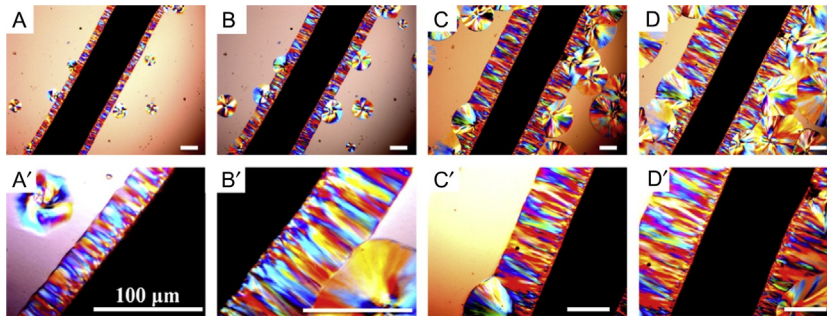

FIG. 11.4 POM observation of the development of transcrystalline morphology of PLA/PEG matrix induced by nanohybrid PLA fiber after isothermal crystallization at 140°C for (A) 5 min, (B) 10 min, (C) 20 min, and (D) 30 min. (A′)–(D′) Illustrates the crystalline morphology of (A)–(D) at higher magnification, respectively. All the bars indicate 100 μm. *Reprinted from C. Chen, et al., Unexpected observation of highly thermostable transcrystallinity of poly(lactic acid) induced by aligned carbon nanotubes, Eur. Polym. J. 63 (2015) 177–185 with permission from Elsevier.*

into incredibly compact lamellae, eventually producing a brush-like TC that strings the central fiber axis and finally after 30 min, the radius of TC reaches up to 157.9 μm. Also several spherulites are observed in the bulk [45].

For fibrous filler that can initiate active nuclei with medium density, an HSK structure with polymer crystal lamellae (kebab) periodically decorating surface of nanofibers or nanotubes and aligning approximately perpendicular to its long axis is created [47–50] (Fig. 11.5).

Zhang et al. [49] investigated NHSK obtained from polyethylene (PE) on CNTs and found that MWNTs were first wrapped by a homogeneous coating of PE with few subglobules, then PE chains epitaxially grew from the subglobule and formed lamellar crystals perpendicular to the carbon nanotube axis. It was postulated that the homogeneous coating plays a key role in the formation of NHSK structures.

HSC structures can be found for the systems with fibrous filler initiating only a few nuclei, which can develop into large polymer spherulites without hindrance. HSC structure with fibrous filler serves as shish, and polymer spherulites as calabash [43,51–53] (Fig. 11.6).

11.4 THERMAL ANALYSIS METHODS IN PNCS CHARACTERIZATION

Thermal analysis methods are widely applied to characterize the thermal properties and behavior of polymer-based nanocomposites and to study effects associated with the presence of nanoparticles dispersed in polymer matrix. In the following sections, application of various thermal analysis method in nanocomposites field will be presented and discussed.

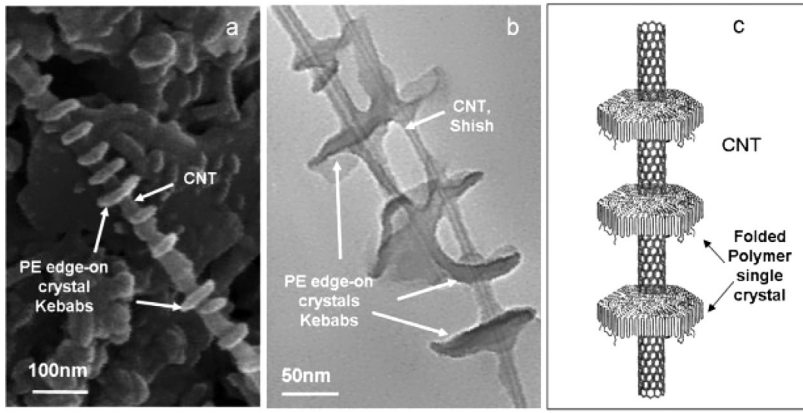

FIG. 11.5 PE/PE/MWCNT NHSK structure produced by crystallization of PE on MWCNTs at 103°C in *p*-xylene for 0.5 h: (A) SEM image shows that MWCNTs are decorated by disc-shaped PE single crystals and PE-functionalized MWCNTs can therefore be achieved. (B) TEM image of enlarged PE/MWCNT NHSK structures. (A) and (B) show that periodicity of the kebabs is ~50–70 nm. (C) Schematic representation of the PE/CNT NHSK structure. For clarity SWNT was used. The PE forms folded lamellar single crystals on the CNT surface with polymer chains perpendicular to the lamellae. *Reprinted from C.Y. Li, et al., Nanohybrid shish-kebabs: periodically functionalized carbon nanotubes, Adv. Mater. 17(9) (2005) 1198–1202 with permission from Wiley.*

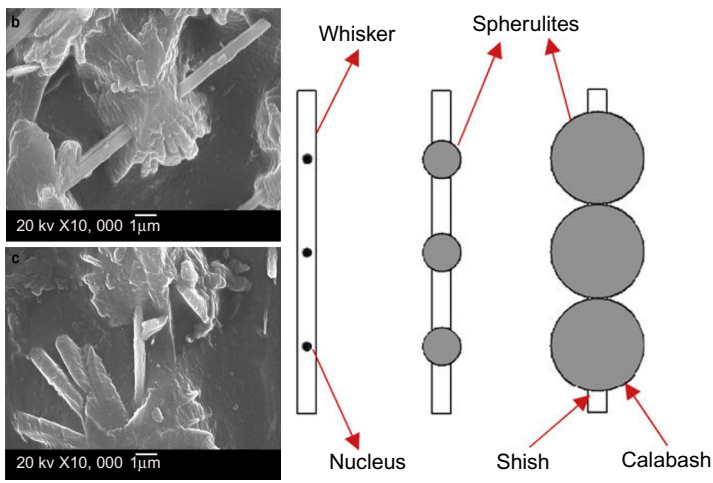

FIG. 11.6 Left: SEM images to represent the crystallization morphology in injection molded bar of PP/SMCW composites (A) and (B) Shish-calabash crystallization morphology observed in the composites. Right: The schematic representation of formation process of shish-calabash crystallization morphology. *Reprinted from N. Ning, et al., Interfacial enhancement by shish–calabash crystal structure in polypropylene/inorganic whisker composites, Polymer 50(15) (2009) 3851–3856 with permission from Elsevier.*

11.4.1 DSC

DSC, introduced in the early 1960s, is a widely used polymer characterization technique. It facilitates the study of melting, crystallization, glass transition, and other effects, which show either changes in heat capacity or a latent heat [54]. The main advantage of DSC is short time of measurement and reasonable accuracy so that it is one of the most frequently used thermal analysis techniques.

11.4.1.1 Melting and Crystallization

Mangal et al. [33] investigated polymer-phase stability in nanocomposites by DSC in the context of the effect of NPs on entanglement dynamics of their host polymer.

They found that favorable enthalpic interactions between the grafted and host chains can be used to overcome the tendency of nanoparticles to phase separate in high molecular weight polymer hosts. Moreover, it has been observed that at a fixed temperature difference from T_g, NPs slow down polymer relaxation on all timescales, including the segmental relaxation time.

Nanocomposites with dynamically asymmetric interphases formed by PMMA (a high-glass-transition temperature polymer), adsorbed on nanoparticles, and poly(ethylene oxide) (PEO) (a low-glass-transition temperature miscible matrix), were postulated by Senses et al. [34] and studied by DSC method. In nanocomposites with PMMA-adsorbed particles, PEO chains interact with PMMA on particle surfaces. In this system, the Rouse rates are identical to PEO homopolymer, contrary to much slower rates observed in highly attractive bare-particle systems.

Hence, Uemura et al. [12] investigated by DSC phase transition of polymers in subnanometer regions by incorporation of PEG into nanochannels of porous coordination polymers (PCPs) (Fig. 11.7).

DSC results show that for the neat PEG sample, an endothermic melting peak at 22°C was found, and no transition was observed for the only host in this entire temperature region. However, **1a** ⊃ PEG clearly exhibited a transition at −36°C, which is much lower than the melting temperature of neat PEG. The peak position and the transition heat for the confined PEG were fairly independent of the amount of PEG loaded in the channels. Moreover, a hysteresis effect was confirmed during heating and cooling scans, indicating that it was a first-order transition.

The thermal properties of polyamide 6 (PA6)/clay nanocomposites were studied by Li and coworkers using DSC technique [55]. It was found that the crystallization behavior of PA6 was significantly influenced by the addition of clay to the polymer matrix (Fig. 11.8).

For pristine PA6, only one endothermic peak ($T_{m,\alpha}$), connected to the melting of α-form crystals of PA6, was found at 225°C, indicating that in the pristine PA6 the α-crystals were the dominant crystalline phase.

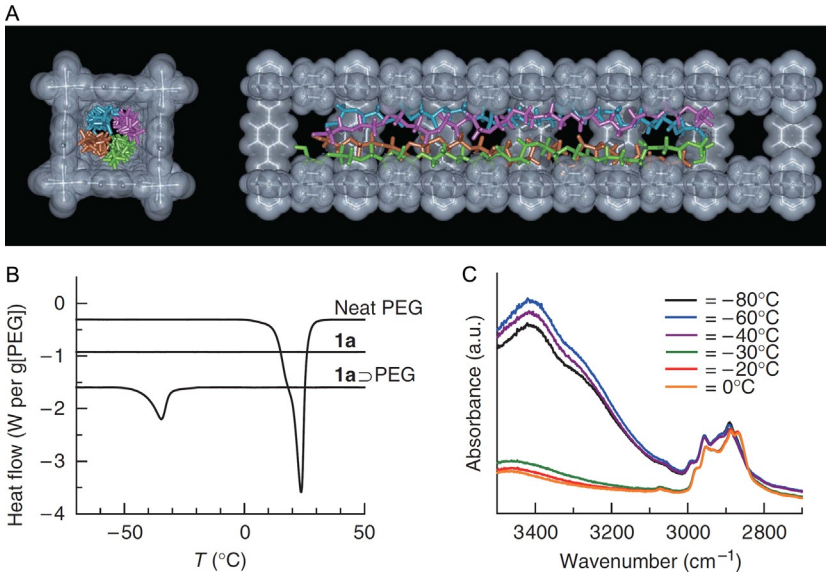

FIG. 11.7 Structure and thermal transition behavior of PEG encapsulated in **1a**. (A) Typical MD structure of PEG 14-mer ($M_w = 634.7$) encapsulated in the subnanometer channel. (B) DSC heating curves of neat PEG, **1a** and **1a** ⊃ PEG. (C) Variable temperature infrared spectra of **1a** ⊃ PEG. M_w of PEG used in these measurements was 600. *Reprinted from T. Uemura, et al., Unveiling thermal transitions of polymers in subnanometre pores, Nat. Commun. 1 (2010) 83 with permission from Nature Publishing Group.*

For PA6 characteristic is second endothermic peak ($T_{m,\gamma}$), corresponding to the melting of the less stable γ-form crystals of PA6 at ca. 215°C as a left shoulder of melting peak. As it was observed on DSC profiles, with increasing clay content, the magnitude of $T_{m,\gamma}$ increased, while the magnitude of $T_{m,\alpha}$ gradually decreased.

Based on these findings authors postulated that the less stable γ-crystals melt at low temperatures during heating, while the stable α-crystals formed freely from polymer chains melt at high temperatures. One more endotherm was found on DSC curve and it was attributed to the melting of the constrained crystals formed within the confined environment of the intercalated clay galleries ($T_{m,4}$) (Fig. 11.9).

Wan et al. [56] investigated melting and crystallization behavior of polypropylene/fullerene C_{60} nanocomposites using DSC method. Rheological investigation results revealed that in the low frequency region, the complex viscosity for PP/C_{60} nanocomposites containing DHBP was much higher than that of pure PP due to chain entanglement effect. The entanglement of polymer chains strongly influences the crystallization process of polymer matrix since the rearrangement of chains is necessary to chain folding and perfection of crystals. However, the initial crystallization temperature and the crystallization

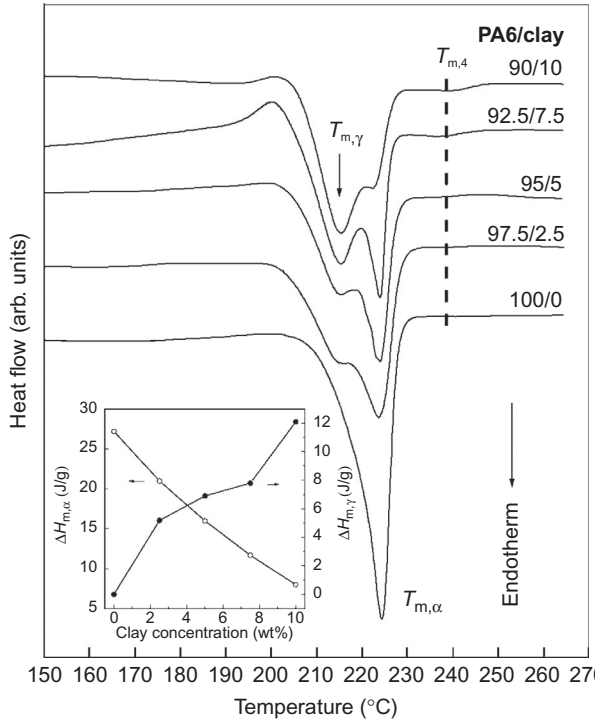

FIG. 11.8 DSC heating curves for neat PA6 and the nanocomposite samples. The inset shows the enthalpies of the melting peaks of both the α- and γ-crystals ($\Delta H_{m,\alpha}$ and $\Delta H_{m,\gamma}$, respectively) as a function of clay concentration (heating rate 10°C/min). *Reprinted from T.-C. Li, et al., Effect of clay addition on the morphology and thermal behavior of polyamide 6, J. Appl. Polym. Sci. 103 (2) (2007) 1191–1199 with permission from Wiley.*

maximum peak temperature of PP/C_{60} nanocomposites containing DHBP increased more than 10°C in comparison to neat PP. This might result from the nucleation effect of branch points on the crystallization of PP chains, while the addition of only C_{60} resulted in slight increases in crystallization temperatures that suggest weak nucleating effect.

Yang et al. [57] studied formation of β-transcrystallinity of PP induced by two-dimensional layered interface in materials with different number of layers obtained by coextrusion of β-nucleated polypropylene (β-PP) and polypropylene (PP). PP is a polymorphic polymer with at least three crystalline forms, that is, the monoclinic α-form, trigonal β-form, and orthorhombic γ-form. In DSC curves for layered specimens, two endothermic melting peaks were observed at ca. 154°C and 167°C connected to the existence of β- and α-crystals [58]. Based on DSC results, the fraction of β-crystals (F_β) in the matrix has been calculated from Eq. (11.3) as

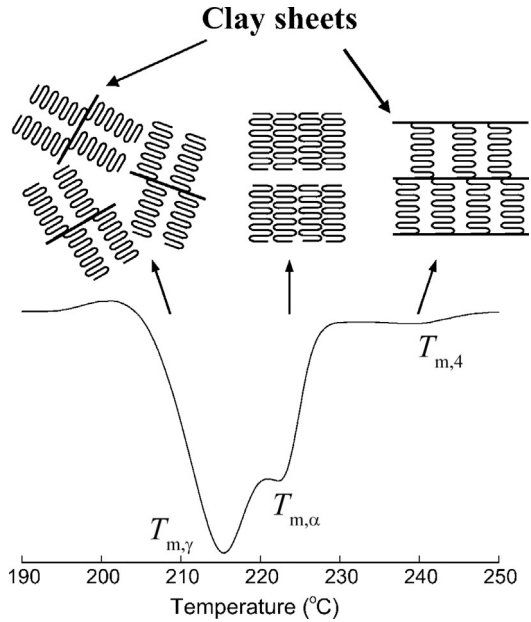

FIG. 11.9 Schematic model of the possible origins of the multiple melting peaks observed in the DSC study of the nanocomposite samples. *Reprinted from T.-C. Li, et al., Effect of clay addition on the morphology and thermal behavior of polyamide 6, J. Appl. Polym. Sci. 103(2) (2007) 1191–1199 with permission from Wiley.*

$$F_\beta = \frac{q}{q + \dfrac{\Delta H_\alpha}{\Delta H_\beta}} \tag{11.3}$$

where ΔH_α and ΔH_β are the enthalpy of melting of α- and β-phase, respectively, determined from the area of the melting peaks. "q" is the ratio between the equilibrium enthalpy of fusion of α- and β-phases.

Two kinds of β-crystals were revealed in microscopic observations in layered samples: β-TC located in PP layers and β-spherulites located in β-PP layers. The content of β-TC ($F_{\beta\text{-TC}}$) can be determined from the relationship:

$$F_{\beta\text{-TC}} = F_\beta - F_{\beta\text{-S}} \tag{11.4}$$

where F_β is the content of β-crystal and $F_{\beta\text{-S}}$ is the content of β-spherulites in layered samples. Results are presented in Table 11.1.

By applying DSC method, melting, crystallization, and nucleation behavior of polyoxymethylene/hydroxyapatite (POM/HAp) nanocomposites have also been investigated [59,60]. On the DSC curves, only one melting peak with maximum at 167°C for pure POM has been observed, while for all POM/HAp nanocomposites, two maximum at 166°C and at 171°C were found. This effect has been explained by the differences in lamellar thickness

TABLE 11.1 Content of β-Crystal and β-TC in Layered Specimens Obtained From DSC and 1D-WAXD

Specimens	DSC		1D-WAXD	
	F_{β} (%)	$F_{\beta\text{-}TC}$ (%)	K_{β} (%)	$K_{\beta\text{-}TC}$ (%)
2-Layer	57.4	10.7	49.6	7.2
4-Layer	67.8	21.1	58.0	15.6
8-Layer	76.9	29.1	65.8	22.4
16-Layer	83.5	36.8	71.4	29.0
32-Layer	87.3	38.1	76.4	31.8
64-Layer	90.4	42.6	81.3	37.9
128-Layer	92.4	44.6	83.4	40.0
Unstratified sample	95.7		86.9	

Reprinted from S. Yang, et al., Formation mechanism and morphology of β-transcrystallinity of polypropylene induced by two-dimensional layered interface, Macromolecules 48(12) (2015) 3965-3973 with permission from American Chemical Society.

due to HAp nucleation effect and the formation of different crystal structures in the presence of HAp. Using DSC results for main melting peak, the lamellar thickness was calculated according to Gibbs-Thomson equation [61,62]:

$$T_{\mathrm{m}} = T_{\mathrm{m}}^{\circ}\left(1 - \frac{2\sigma_{\mathrm{e}}}{\Delta h_{\mathrm{o}} l}\right) \tag{11.5}$$

where T_{m}° is the equilibrium melting temperature, Δh_{o} is thermodynamic enthalpy of fusion per unit volume of the crystalline phase, and σ_{e} is the free surface energy of the end faces lamellar that is associated with the crystallization process.

It has been observed that for the first heating run lamellar thickness calculated from the first maximum decreases to 9.1 nm with the increase of HAp content to 2.5% and then again increases to 9.5 for POM/5.0% HAp. Calculated from the DSC results the degree of crystallinity increased for POM/0.5% HAp composite and decreased for POM/1.0% HAp and POM/2.5% HAp. This effect was attributed to the influence of HAp nanoparticles on the crystallization process of POM—Hap act as effective nucleating site and lead to the higher degree of crystallinity for 0.5% and 1.0% HAp, but further increases of HAp content leads to hindering of the crystallization process by disturbing growing fronts, and the degree of crystallinity becomes lower, as well as crystals smaller and more defected [41,60].

PEO nanofiber mats with biobased cellulose nanocrystals (CNCs) and cellulose nanofibrils (CNFs) as reinforcement were produced using electrospinning by Xu et al. [63] who studied by DSC the effects of the CNCs and CNFs on the melting and crystallization of PEO nanofibers. They observed a unique shish-kebab-like crystalline structure in both pure and filled PEO nanofibers (Fig. 11.10).

Generally, neat PEO exhibits one single melting peak at ca. 68°C, while pure nanofiber exhibits a broader melting region that can be separated into two peaks (at 66.3°C and 71.9°C). For electrospun polymer nanofibers double-melting peak has been reported and it has been attributed to the coexistence of lamellar crystals and extended chain crystals [64]. For the electrospun nanofibers containing CNCs or CNFs, broadened double melting peaks were recorded, indicating similar coexistence of nonoriented and oriented crystals (Fig. 11.11).

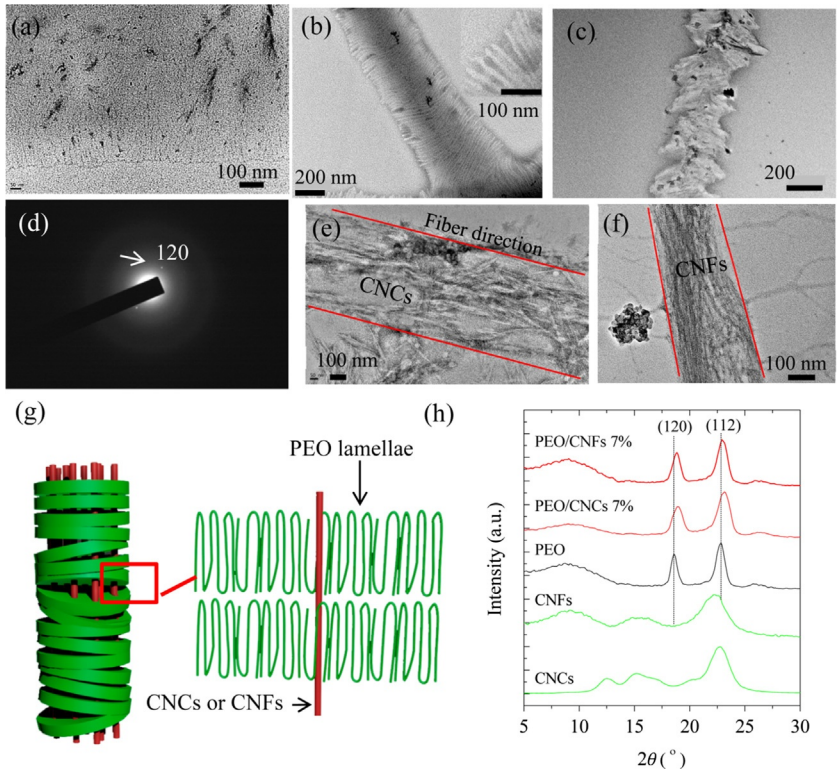

FIG. 11.10 (A) TEM images of pure PEO nanofibers; (B) PEO/CNF 4% nanofibers; (C) PEO/CNF 4% nanofiber after mild water etching; (D) SAED pattern taken from (B); (E) PEO/CNC 4% and (F) PEO/CNF 4% nanofibers after PEO removal; (G) illustration of the shish-kebab-like structure; (H) WAXD patterns of PEO/CNC and PEO/CNF 7% nanofibers. *Reprinted from X. Xu, et al., Comparison between cellulose nanocrystal and cellulose nanofibril reinforced poly(ethylene oxide) nanofibers and their novel shish-kebab-like crystalline structures, Macromolecules 47(10) (2014) 3409–3416 with permission from American Chemical Society.*

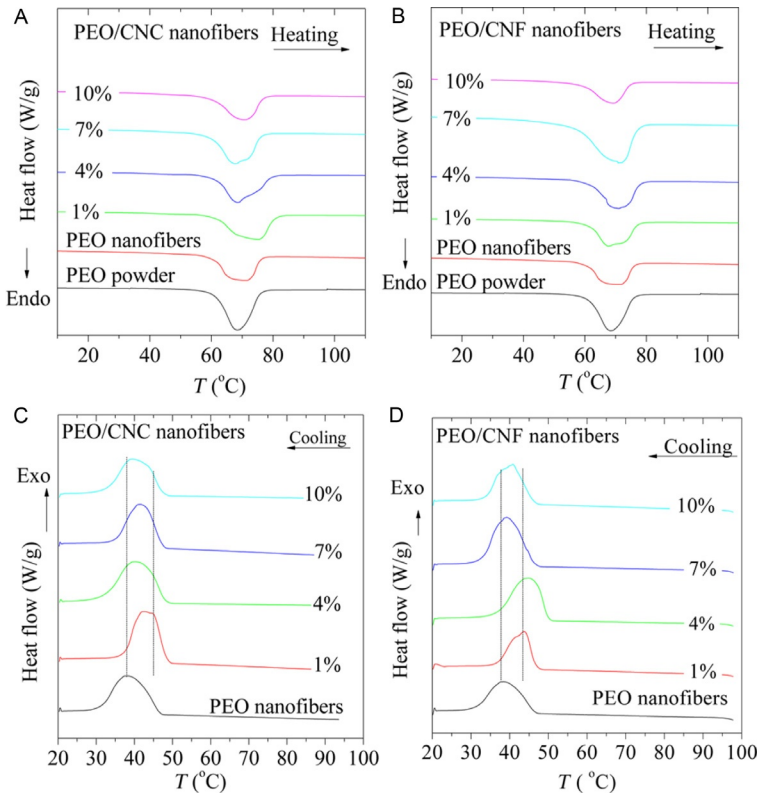

FIG. 11.11 DSC thermograms for the melting and nonisothermal crystallization of PEO/CNC and PEO/CNF nanofibers: (A) PEO/CNC melting; (B) PEO/CNF melting; (C) PEO/CNC crystallization; (D) PEO/CNF crystallization. *Reprinted from X. Xu, et al., Comparison between cellulose nanocrystal and cellulose nanofibril reinforced poly(ethylene oxide) nanofibers and their novel shish-kebab-like crystalline structures, Macromolecules 47(10) (2014) 3409–3416 with permission from American Chemical Society.*

The double melting was suppressed at 10% content of CNCs or CNFs, due to high concentration of nanoparticles that hinders the PEO crystals growth. It was also found that the melting temperatures of PEO/CNCs are higher than those of PEO/CNFs; possible explanation could be higher perfection of the shish-kebab-like structure in the former.

11.4.1.2 Exfoliation and Intercalation

Hutchinson and coworkers [65,66] applied DSC to identify the different reactions of homopolymerization and cross-linking that occur in the intra- and extra-gallery regions of polymer/layered silicate (PLS) nanocomposites. From literature it is known that in order to obtain a high degree of exfoliation, the intragallery curing reaction must occur before the extra-gallery curing,

otherwise, when the extra-gallery reaction occurs first, the network formed in the bulk of the nanocomposite prevents further nanostructural development of exfoliated clay galleries [67–69a]. Authors investigated curing of epoxy resin (EP) in the presence of MMT by using DSC method and confirmed the obtained structures by transmission electron microscopy (TEM) and SAXS methods. They found for the DGEBA/MMT/Jeffamine system a shoulder on the high-temperature flank of the nonisothermal DSC cure curve, which was attributed to the intragallery homopolymerization reaction. It occurs after the extra-gallery cross-linking reaction, which is too late and in consequence the exfoliation is inhibited (Fig. 11.12).

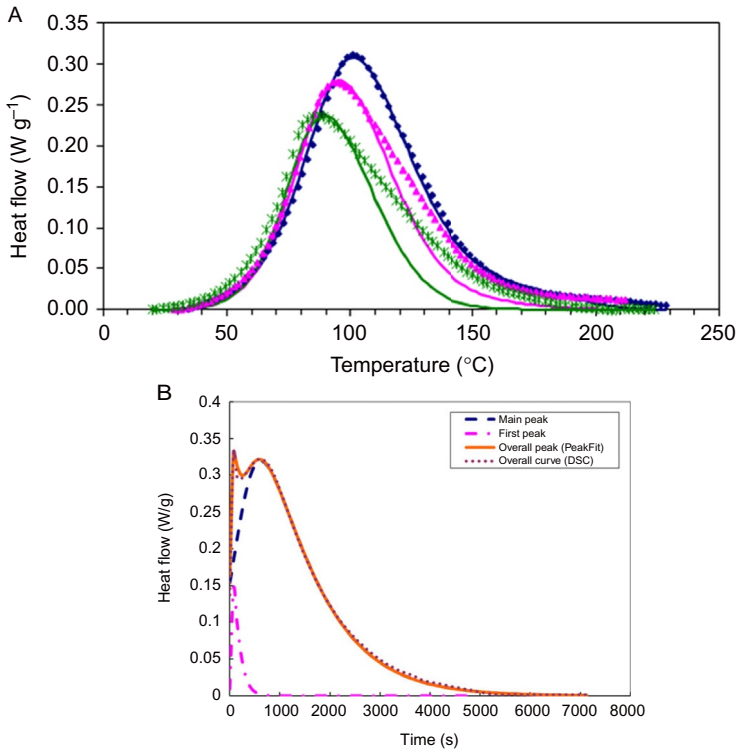

FIG. 11.12 (A) DSC cure curves at 2.5 K/min heating rate for the DGEBA-Jeffamine system with the following clay contents: without clay *(filled diamond)*; 10 mass% *(filled triangle)*; 20 mass% *(asterisk)*. The full lines represent the fit of the autocatalytic model. Exothermic direction is upward, and specific heat flow is referred to the total sample mass, including clay. (B) Peak separation using PeakFit program showing comparison of the fitted curve with DSC data for sample TGAP/DDS/MMT (5 wt%) cured at 165°C for 2 h. *(A) Reprinted from F. Shiravand, et al., Thermal analysis of polymer layered silicate nanocomposites, J. Therm. Anal. Calorim. 118(2) (2014) 723–729. (B) Reprinted from F. Shiravand, J.M. Hutchinson, Y. Calventus, Influence of the isothermal cure temperature on the nanostructure and thermal properties of an epoxy layered silicate nanocomposite, Polym. Eng. Sci. 54(1) (2014) 51–58.*

For another system, it was observed that the intragallery reaction in isothermal cure occurs before the extra-gallery crosslinking reaction (Fig. 11.12B). That implies that there should be better conditions for more efficient exfoliation as confirmed by SAXS, which shows no scattering peaks, and by TEM, which shows rather randomly distributed clay layers with essentially no layer stacking.

11.4.1.3 Glass Transition, Relaxation, and Fictive Temperature

The effect of the addition of organo-modified MMT on the structural relaxation phenomena of poly(ethylene terephthalate)/poly(cyclohexanedimethanol terephthalate) copolymer (PET/PCHDMT) was studied by means of DSC in the work of Greco et al. [70]. It has been observed that the relaxation behavior depends on both the MMT and organic modifier—the organic modifier acts as a plasticizer causing a decrease in glass-transition temperature and increase in the specific heat discontinuity at the glass transition. On the contrary, the addition of the nanofiller leads to an increase of the glass-transition temperature, due to an enhanced confinement of relaxation, and a decrease of the specific heat discontinuity that has been linked with an increase of the content of rigid amorphous phase. Based on DSC data the fictive temperature and relaxation time were determined. The fictive temperature is the so-called true glass-transition temperature of an aged polymer [71,72], which represents the temperature at which the glass in this configuration would be at equilibrium. Fictive temperature is one of the parameters in the Tool-Narayanaswamy-Moynihan equation [73–75] and is widely used for characterization of glassy materials.

The usual procedure for determining the fictive temperature is by the "equal areas" method from the DSC curves [71,75,76]. One of the fundamental advantages of the concept of fictive temperature is that it can define the state of the glass also after whatsoever thermal history [72]. Moreover, from the DSC data it is possible to calculate the fragility index m. Calculation of the fragility index from the slope of $\log_{10}\tau$ vs T_g/T curve at the glass transition was proposed by Ngai and Rendell [77], and it is defined as

$$m = \left.\frac{d\log_{10}\tau}{d\left(T_g/T\right)}\right|_{T=T_g} \tag{11.6}$$

where τ is relaxation time.

However, for calculation of fragility index the knowledge of the relaxation time dependence over T is necessarily based on Tool-Narayanaswamy-Moynihan equation [73–75]:

$$\tau = \tau_0 \exp\left(\frac{x\Delta h^*}{RT}\right)\exp\left[\frac{(1-x)\Delta h^*}{RT_f}\right] \tag{11.7}$$

where τ_0 is the preexponential factor, x the nonlinearity parameter, Δh^* the apparent activation enthalpy, R the gas constant, and T_f, the fictive temperature.

Flory et al. [78] investigated the glass-transition temperature, enthalpy relaxation during physical aging and fragility of PMMA/single wall carbon nanotubes nanocomposites using DSC. Generally, relaxation process of polymers is a result of the nonequilibrium state of the polymer below the glass-transition temperature. Polymer glasses are nonequilibrium materials and their physical and mechanical properties evolve with time to reach the equilibrium state through rearrangement of polymer segments. Such effect is called structural relaxation or physical aging [79]. Authors investigated enthalpy relaxation behavior during isothermal aging at T_g and at temperature 2°C lower than the glass-transition temperature—DSC curves are presented in Fig. 11.13.

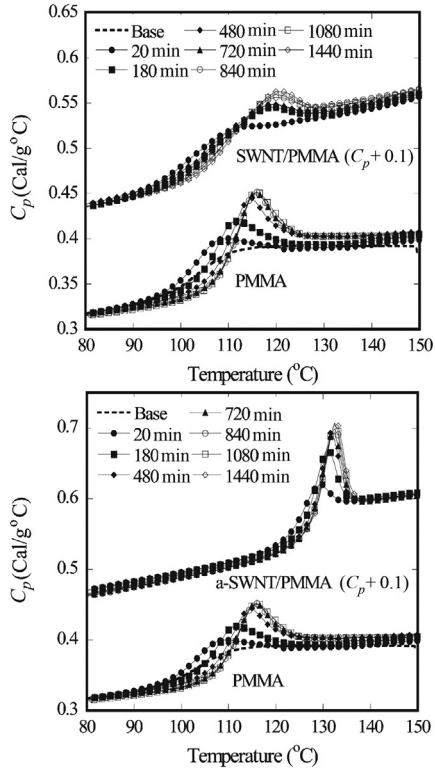

FIG. 11.13 DSC scans of the heat capacity versus temperatures for PMMA, SWNT/PMMA, and amino functionalized-SWNT/PMMA (a-SWNT/PMMA) after isothermal annealing at the respective T_g for various aging times. *Reprinted from A.L. Flory, T. Ramanathan, L.C. Brinson, Physical aging of single wall carbon nanotube polymer nanocomposites: effect of functionalization of the nanotube on the enthalpy relaxation, Macromolecules 43(9) (2010) 4247–4252 with permission from American Chemical Society.*

Authors revealed that very small amounts of a-SWNTs added to PMMA caused significant increase of the glass transition, but the extent of physical aging significantly decreased in a-SWNT/PMMA compared with neat PMMA. Moreover, the activation energy of the relaxation process and the fragility index in PMMA and a-SWNT/PMMA are comparable. However, incorporation of single-wall carbon nanotubes (SWNTs) into PMMA matrix does not change the glass-transition temperature of polymer. Additionally, the results show slower approaches to equilibrium for both functionalized and unfunctionalized nanotubes in PMMA.

11.4.1.4 Kinetics

DSC was also used to investigate the thermal behavior of virgin PS and PS/clay nanocomposites and to calculate isoconversional kinetic of the melting process. It was revealed that the activation energy did not depend on the conversion for the gels prepared under isothermal conditions, whereby for the gels prepared under continuous cooling conditions an increase in the activation energy with degree of conversion was observed [80].

PET glycol/MMT nanocomposites with different filler contents were investigated by Saiter et al. [81] using DSC and temperature modulated differential scanning calorimetry (TMDSC). Authors determined the values of the fragility index *m:*

$$m = \frac{\Delta h^*}{RT_g \ln 10} \tag{11.8}$$

and calculated the average size of a cooperative rearranging region (CRR) by the quantity $z(T_g)$ at the glass transition according to the relationship proposed by Solunov [82]:

$$z(T_g) = \frac{T_g}{T_g - T_k} \tag{11.9}$$

where T_k is the Kauzmann temperature. Average number of monomer units by CRR noted N_α, have been calculated using the method developed by Donth [83]. The results show that the presence of MMT in PET matrix influences structural relaxation phenomena. From the results obtained it was found that up to 3% MMT, the amorphous phase formed by PET chains is more constrained by MMT, involving a decrease of m and N_α, while at 5% MMT content a partial phase separation occurs and the polymer chains gain mobility that leads to an increase of m and N_α [81].

11.4.1.5 Crystalline Fraction (CF), Rigid Amorphous Fraction (RAF), and Mobile Amorphous Fraction (MAF)

Another example of application of DSC for characterization of PNCs was presented in the work by Klonos and Pissis [84]. They applied DSC, dielectric

spectroscopy (DRS) with scanning electron microscopy (SEM) to study effects of filler on crystallization, glass transition, and segmental dynamics and on the amount of the various polymer fractions such as crystalline fraction (CF), rigid amorphous fraction (RAF), and mobile amorphous fraction (MAF) in PLLA/fumed silica nanocomposites. The authors followed thermal protocols: (A) the sample under investigation was heated up to 200°C for erasing thermal history; it was then cooled rapidly at ~100 K/min down to 0°C, and again heated up to 200°C with heating rate 10 K/min; (B) for isothermal crystallization to study crystallinity induced effects next to those imposed by the filler, the sample was melted by heating up to 200°C, cooled rapidly down to 115°C, and then isothermal annealed for 30 min. After annealing, the sample was again cooled rapidly and then heated from 0 to 200°C at 10 K/min for the evaluation of glass transition and melting process. In the DSC curves (Fig. 11.14), the glass transition at about 60°C, cold crystallization at about 100 and 160°C (the second preceding melting), and melting at about 180°C can be seen.

From DSC curves obtained according to protocol for the initially amorphous samples (A), glass-transition temperature, T_g, the heat capacity step at glass transition, ΔC_p, and the temperatures and enthalpies of cold crystallization (T_{cc}, ΔH_{cc}) and of melting (T_m, ΔH_m) were determined. From protocol (B) for the semicrystalline (annealed) samples, evaluation of T_g, ΔC_p and the enthalpy and temperature position of melting peaks (ΔH_m, T_m) was performed.

Next, CF was calculated from Eq. (11.10).

$$\mathrm{CF} = \frac{\Delta H_m - \Delta H_{cc}}{(1 - f_{\mathrm{filler}})\Delta H^{\mathrm{PLLA}}_{100\%\mathrm{cryst}}} \tag{11.10}$$

where f_{filler} is the filler fraction and $\Delta H^{\mathrm{PLLA}}_{100\%\mathrm{cryst}}$ is the theoretical enthalpy of melting for 100% crystalline PLLA.

For calculation of MAF and RAF, the following equations were employed:

$$\Delta C_{p,\mathrm{n}} = \frac{\Delta C_{p,\mathrm{DSC}}}{(1 - f_{\mathrm{filler}})(1 - \mathrm{CF})} \tag{11.11}$$

$$\mathrm{MAF} = \frac{\Delta C_{p,\mathrm{n}}}{\Delta C^{\mathrm{PLLA}}_{p,\mathrm{amorph}}}(1 - \mathrm{CF}) = \frac{\Delta C_{p,\mathrm{n}}}{0.56(\mathrm{J/g\ K})}(1 - \mathrm{CF}) \tag{11.12}$$

$$\mathrm{RAF}_{\mathrm{total}} = 1 - \mathrm{MAF} - \mathrm{CF} \tag{11.13}$$

where $\Delta C_{p,\mathrm{DSC}}$ is the measured heat capacity change at glass transition as taken from DSC, $\Delta C_{p,\mathrm{n}}$ the heat capacity change of PNCs normalized to the amorphous polymer mass, $\Delta C^{\mathrm{PLLA}}_{p,\ \mathrm{amorph}}$ is the amorphousneat PLLA [85]. The factor "1 − CF" has been inserted in Eq. (11.11), as MAF and $\mathrm{RAF}_{\mathrm{total}}$ refer to the whole polymer mass (validity of Eq. 11.12); without this factor, MAF and $\mathrm{RAF}_{\mathrm{total}}$ would refer to the amorphous polymer.

Authors did not observe any significant changes in the glass-transition temperature caused by the filler using DSC, whereas the heat capacity step decreases in the PNCs. They revealed that $\mathrm{RAF}_{\mathrm{filler}}$ increased with filler

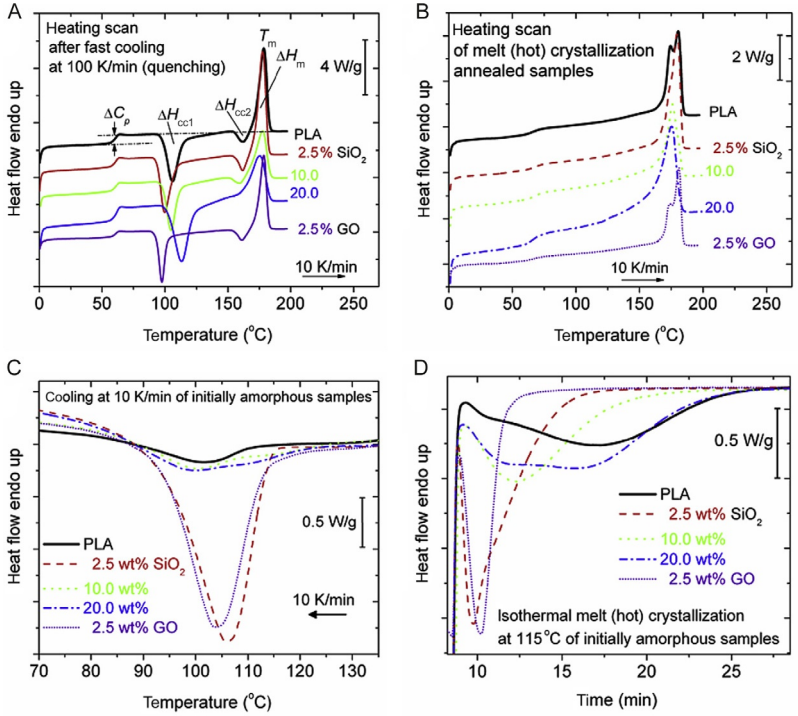

FIG. 11.14 (A, B) DSC heating thermograms for the samples and the conditions of measurement indicated on the plots. Indicated on the plot are also the various events recorded, along with characteristic values: glass transition (ΔC_p), cold crystallizations ($\Delta H_{cc1,2}$), and melting of crystals (ΔH_m, T_m). The curves are normalized to sample mass. (C) DSC cooling thermograms at 10 K/min in the temperature range of nonisothermal crystallization of initially amorphous samples. (D) DSC heat flow vs time during isothermal melt (hot) crystallization annealing at 115°C for the same initially amorphous samples. *Reprinted from P. Klonos, P. Pissis, Effects of interfacial interactions and of crystallization on rigid amorphous fraction and molecular dynamics in polylactide/silica nanocomposites: a methodological approach, Polymer 112 (2017) 228–243 with permission from Elsevier.*

fraction, with a saturation for the largest loading (20 wt%), assigned to filler aggregation confirmed by morphological characterization. Moreover, $RAF_{crystal}$ and MAF values stayed within experimental error almost constant with increasing filler load (Fig. 11.15).

The obtained results indicate that interfacial interactions (RAF_{filler}) in combination with changes in semicrystalline morphology dominate polymer dynamics in semicrystalline PNCs [84].

11.4.2 TMDSC

Differential scanning calorimetry with temperature modulation (TMDSC) is an extension to conventional DSC. In this technique on conventional linear

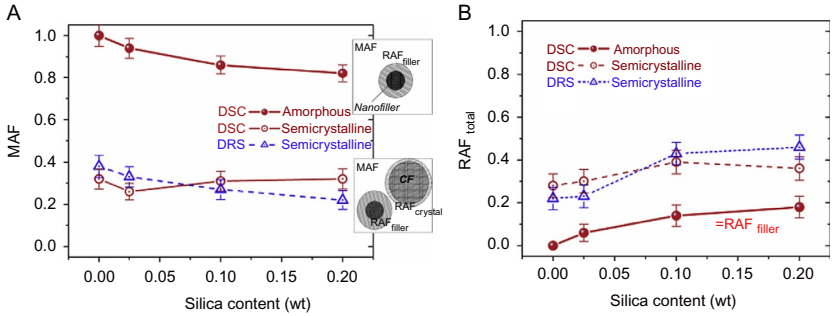

FIG. 11.15 (A) mobile, MAF, and (B) total rigid amorphous fraction, RAF_{total}, for PLLA and PLLA PNCs as obtained by DSC (Eqs. 11.3, 11.4) against filler loading. Results are shown for amorphous (quenched) and semicrystalline (annealed at 115°C) samples. The schemes on the right in (A) provide simplified models for the various polymer fractions in (top) amorphous (two-phase model, MAF/RAF) and (bottom) semicrystalline samples (three-phase model, MAF/RAF/CF). For comparison, respective results by DRS have been included. *Reprinted from P. Klonos, P. Pissis, Effects of interfacial interactions and of crystallization on rigid amorphous fraction and molecular dynamics in polylactide/silica nanocomposites: a methodological approach, Polymer 112 (2017) 228–243 with permission from Elsevier.*

and constant heating program a periodically varying sinusoidal temperature modulation is superimposed [86].

After application of a mathematical treatment to the raw data it can be deconvoluted to obtain the sample response to the perturbation from its response to the underlying heating program; in this way the reversible and irreversible nature of a thermal event can be probed. The main advantage of TMDSC is disentangling overlapping phenomena, improving resolution, and enhancing sensitivity [87].

In the 1990s, Reading et al. [87–89] applied TMDSC to the study of polymers and their phase transitions. They showed that by using this technique it is possible to separate reversing phenomena like glass transition or partial melting from nonreversing processes, for example, relaxation or recrystallization, in one measurement. As frequency dependence in TMDSC measurements was found in the glass-transition region [90], TMDSC data treatment with frequency-dependent complex heat capacity was proposed by Schawe [91]. In 2006, a new multi-frequency TMDSC with stochastic temperature modulation TOPEM was introduced [92].

11.4.2.1 Glass Transition

TMDSC studies on PNCs are vast. Along this line of interest, Holt et al. [93] compared the properties of poly(2-vinylpyridine)/silica-based nanocomposites with polymer chains covalently bonded (PGNs) or physically adsorbed (PNCs) to these silica nanoparticles. The glass-transition region was investigated using TMDSC method (Fig. 11.16).

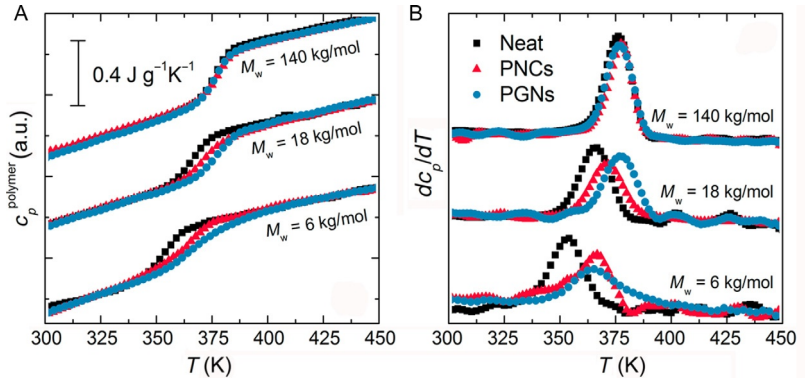

FIG. 11.16 (A) Specific heat capacity from calorimetry illustrating the glass transition of the matrix component for the polymer nanocomposites and polymer-grafted nanoparticles for each molecular weight. (B) Derivative of specific heat capacity to better demonstrate the broadening of the glass transition in the form of a peak. All curves are arbitrarily vertically shifted for clarity. *Reprinted from A.P. Holt, et al., Controlling interfacial dynamics: covalent bonding versus physical adsorption in polymer nanocomposites, ACS Nano 10(7) (2016) 6843–6852 with permission from American Chemical Society.*

T_g, for both PNCs and PGNs, depended on M_w and relative silica concentration; however, both for PNC and PGNth shift in T_g was negligible, almost coincided with T_g of neat polymer. Moreover, the intermediate average molar mass systems showed a clear change in T_g while the low average molar mass samples displayed a much stronger change in the glass-transition region. Changes in glass transition were also manifested by widening the temperature range that can be clearly seen from the derivative the TMDSC curves (Fig. 11.16B).

Authors postulated that this increase indicates that the segmental mobility has a large gradient, and a significant amount of the segmental mobility is slower than the average mobility.

A detailed study of PNCs with well-dispersed, small (diameter $\sim$1.8 nm) POSS derivative (OAPS) nanoparticles and comparison to conventional PNCs with silica ($D \sim$ 10–50 nm) nanoparticles were performed by Cheng et al. [94]. Based on TMDSC measurements they provided thermodynamic estimates of T_g; there were no transition steps in conventional DSC data of neat OAPS for $T = 313$–453 K. T_g, defined as the midpoint of the transition step, shifts from 372 to 407 K (Fig. 11.17).

An extraordinarily large increase of T_g compared to conventional PNCs with similar loading was observed—P2VP/SiO_2 exhibited T_g shifts of only $\sim$2–5 K while for P2VP/OAPS it was almost 35 K. The ΔC_p of the P2VP/OAPS PNCs remained almost constant at the level $\sim$0.27 J/(g K) despite a strong decrease in polymer weight fraction, which is again in qualitative contrast to conventional PNCs where ΔC_p scales well with polymer fraction (Fig. 11.18).

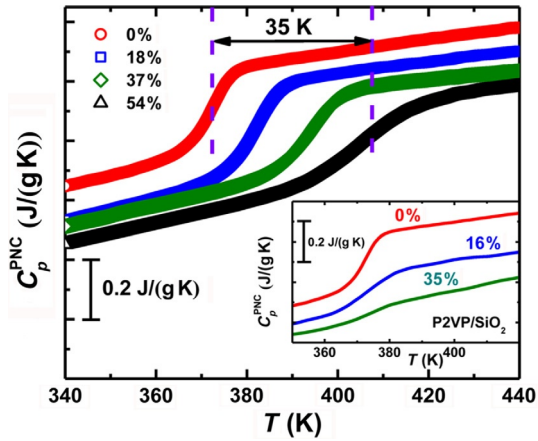

FIG. 11.17 TMDSC measurement data of poly(2-vinylpyridine) (P2VP)/OAPS nanocomposites with different loadings. Inset shows results for P2VP/SiO_2 with NP $D \sim 25$ nm ($\varphi SiO_2 = 0$, 16, and 35 vol%). *Reprinted from S. Cheng, et al., Big Effect of small nanoparticles: a shift in paradigm for polymer nanocomposites, ACS Nano 11(1) (2017) 752–759 with permission from American Chemical Society.*

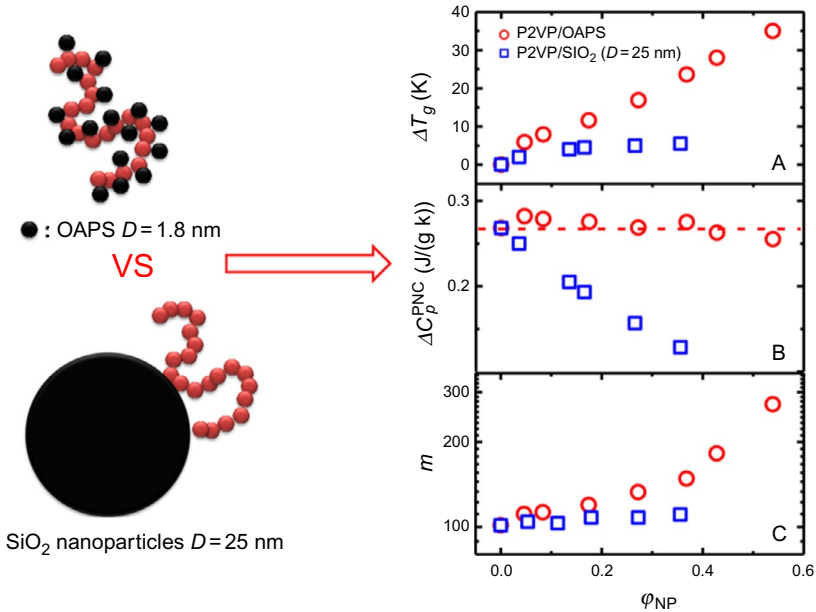

FIG. 11.18 (A) Shift in the glass-transition temperature, ΔT_g, (B) specific heat capacity jump ΔC_p^{PNC} at T_g, and (C) fragility index m as a function of loading for P2VP/OAPS and P2VP/SiO_2 ($DSiO_2 = 25$ nm). *Reprinted from S. Cheng, et al., Big Effect of small nanoparticles: a shift in paradigm for polymer nanocomposites, ACS Nano 11(1) (2017) 752–759 with permission from American Chemical Society.*

Moreover, it was found that calculated fragility index m remarkably grows from 100 for neat P2VP to 270 for φOAPS = 54 vol% compared to a small ~10% change observed in P2VP/SiO_2 PNCs. It should be noted that $m = 270$ is much higher than any value ever reported for polymer melts implying a sharp slowing down of dynamics with cooling and an unusual glass formation behavior of PNCs with small attractive NPs [94].

11.4.2.2 Confinement Effect

Barroso-Bujans et al. [95,96] investigated the effect of the confinement of PEO in porous materials on the crystallization and modification of the glass transition. Materials with 2D-polymer intercalation into graphite oxide (GO) and by surface polymer adsorption onto partially reduced and exfoliated GO (pR-GO) and in graphene sheets (G) were obtained. Three distinct cases of spatial confinement: (i) subnanometer 2D confinement; (ii) frustrated absorption; and (iii) surface immobilization, were distinguished (Fig. 11.19).

Based on spectroscopic results, it was found that in the confined polymer phase a preferential chain conformation is planar zigzag (trans-trans-trans), whereby confined PEO chains are unable to either crystallize or display a calorimetric glass transition. In TMDSC measurements, no signs of calorimetric glass or melting transitions of PEO chains in 2D-confinement in PEO/GO

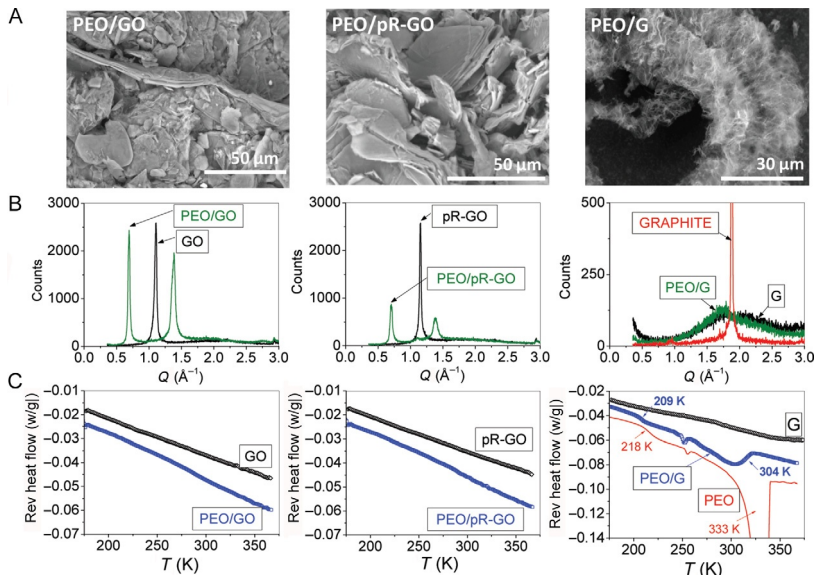

FIG. 11.19 (A) SEM, (B) XRD, and (C) TM-DSC measurements for PEO/GO, PEO/pR-GO, and PEO/G. *Reprinted from F. Barroso-Bujans, et al., Macromolecular structure and vibrational dynamics of confined poly(ethylene oxide): from subnanometer 2D-intercalation into graphite oxide to surface adsorption onto graphene sheets, ACS Macro Lett. 1(5) (2012) 550–554 with permission from American Chemical Society.*

and PEO/pR-GO materials were detected, whereas clear signatures of glass (209 K) and melting transitions (304 K) for the PEO/G sample was found but at temperatures lower than those of bulk PEO. It was postulated that 2D-confined polymer-phase transitions associated with the bulk are inhibited by geometric constraints leading to a lack of cooperation between vicinal polymer chains.

11.4.2.3 Activation Energy of Glass Transition

Vyazovkin group [97] calculated the activation energy of the glass transition for PS/clay systems from the frequency dependence of T_g determined in TOPEM DSC measurements using equation:

$$E = -R\frac{\mathrm{d}\ \ln f}{\mathrm{d}T_g^{-1}} \tag{11.14}$$

E for the glass transition can be determined from the slopes of $\ln f$ vs $1/T_g$. Nanocomposites demonstrated larger value of E than neat PS; it was postulated that an increase in E is related to the effect of nanoconfinement of PS chains in the nanocomposites.

11.4.3 Fast Scanning Calorimetry

Differential fast scanning calorimetry (DFSC) is a relatively new technique developed by Zhuravlev and Schick [98,99]. It is an attractive tool to study kinetics, thermodynamics, and phase transitions of materials that are in the state far from thermodynamic equilibrium. In DFSC, the measurements can be performed at controlled cooling and heating rates between 1 and 100,000 K/s [100].

Schick group employed DFSC to study the temperature range of heterogeneous nucleation caused by both silver nanoparticles and multiwalled carbon nanotubes (MWCNTs) in poly(butylene succinate) (PBSu) nanocomposites [101]. It was found that on cooling from the melt the pristine PBSu did not crystallize at rates higher than 70 K/s, while the nanocomposites needed rates of 500 and 300 K/s for silver and MWCNT, respectively (Fig. 11.20).

Based on DFSC measurements the critical cooling rate for avoiding crystallization was estimated as 70, 300, and 500 K/s for PBSu, PBSu/MWCNT, and PBSu/Ag, respectively, and below 280 K homogeneous nucleation overturns nucleation by the nanoparticles. PBSu and its nanocomposites show a very fast recrystallization kinetics while isothermal crystallization at comparable temperatures is about two orders of magnitude slower. Interestingly, it was observed that the tiny crystals formed at annealing below T_g, melt at 265 K, where overall crystallization from the melt is already one order of magnitude slower than at 320 K, which is the temperature where the recrystallized crystals melt.

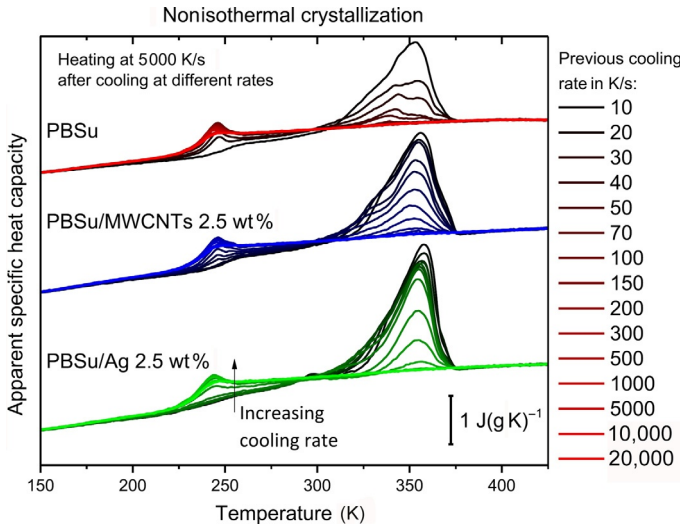

FIG. 11.20 Apparent heat capacity of PBSu and nanocomposites after cooling with various cooling rates and immediate heating at 5000 K/s. The color code on the legend corresponds only to the top panel graph for brevity reasons, however the general remark is that the darker the color of the curve, the lower the cooling rate. *Reprinted from D.G. Papageorgiou, et al., Kinetics of nucleation and crystallization in poly(butylene succinate) nanocomposites, Polymer 55(26) (2014) 6725–6734 with permission from Elsevier.*

11.4.4 LTA Micro-TA

One of the key points in developing and design a new class of nanocomposites with improved properties is understanding the structural and thermomechanical properties of mixed-phase at the nanoscale. LTA, based on atomic force microscopy (AFM) with a heated tip, makes it possible to measure the nanoscale thermal properties of dual-phase polymeric materials [102,103].

In the earlier papers, LTA with the thermally active probe made from a bent piece of Wollaston wire that formed a Pt/Rh heater tip having a lateral topographic resolution on the order of 1 μm were used. Then, Nelson and King proposed batch-fabricated silicon probes with integrated heaters and oxide-sharpened tips with radius of curvature less than 20 nm, which enables to achieve a spatial resolution of about 100 nm [104]. Such a kind of equipment allows to investigate nanosized structures including PNCs. Another extension of LTA method is BE-NanoTA in which periodic heating of the tip surface junction causes periodic local thermal expansion of the substrate. In BE-NanoTA the tip is periodically heated, which enables determination of the mechanical properties of the material, such as Young's modulus and viscoelasticity, by measuring changes in the amplitude and resonance frequency in the function of temperature [105].

LTA technique was applied by Souier et al. [102] who investigated the nanoscale thermal properties of a dual-phase cellulose/polyethylene oxide (PEO) blend (Fig. 11.21) and concluded that LT technique is a robust, nondestructive method for the characterization of thermomechanical properties of polymeric nanocomposites.

By using LTA, it was possible to measure glass transition, melting points, and decomposition temperature of cellulose. Moreover, dehydration of bonded water, which was of interest in terms of water absorption and retention capability of a material, could be analyzed. If LTA is coupled with a constant indentation technique, it not only allows the assignment of the surface phase but also quantifying of their size within a multiphase structure.

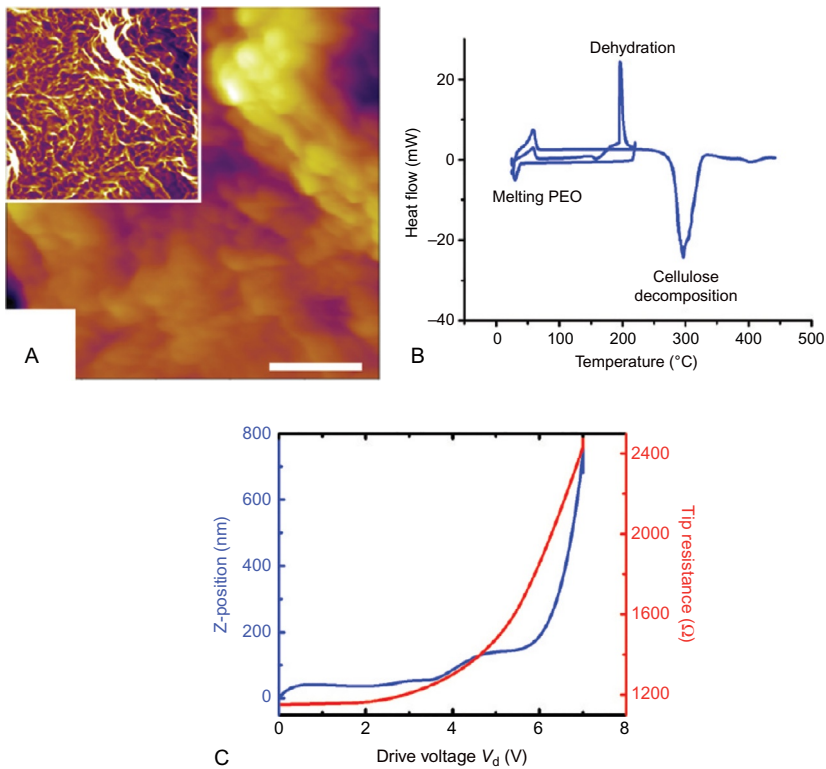

FIG. 11.21 (A) AFM height and phase (in inset) maps on composite PEO/Cel (the scale bar = 250 μm), (B) macroscopic thermal analysis with DSC, and (C) corresponding nanoscopic LTA measurements. *Reprinted from T. Souier, et al., Nanoscale thermal analysis of multiphase polymer nanocomposites, J. Phys. Chem. C 116(15) (2012) 8849–8856 with permission from American Chemical Society.*

11.4.5 Thermogravimetry (TG)

TGA is a well-known and widely used method to determine the weight change characteristics of the investigated samples during heating and associated reaction kinetics [106,107]. In polymeric materials, it is mainly used for studying degradation behavior, but it can also be applied for determination quantity of impurities, additives, or solvent residues. TG is widely used to investigate the influence of nanoadditives on the thermal stability of PNCs.

11.4.5.1 Thermal Stability

Incorporation of nanoparticles to polymer matrix often changes its thermal stability [1,108]. Hence, in cross-linked polyethylene/MWCNTs/nanodiamonds (PEX/MWCNTs/NDs) system progressive significant thermal stability enhancement was observed (Fig. 11.22), and this effect was attributed to the formation of more nanoconfined regions around the nanofillers, in which the local density fluctuations and hindered macromolecular chain mobility lead to a decrease of chemical reactivity [109].

Abraham et al. [110] investigated highly modified CNCs, acetylated cellulose nanocrystals (Ac-CNC) and epoxy-CNC nanocomposites; significant enhancement of thermal stability CNC after acetylation was observed (Fig. 11.23).

The small weight loss initially, at the temperature range 100–150°C for CNC has been attributed to the evaporation of physically bound moisture. DTG peaks observed between 240°C and 280°C correspond to the thermal degradation of CNC and a small wide dip was observed between 310°C and 450°C.

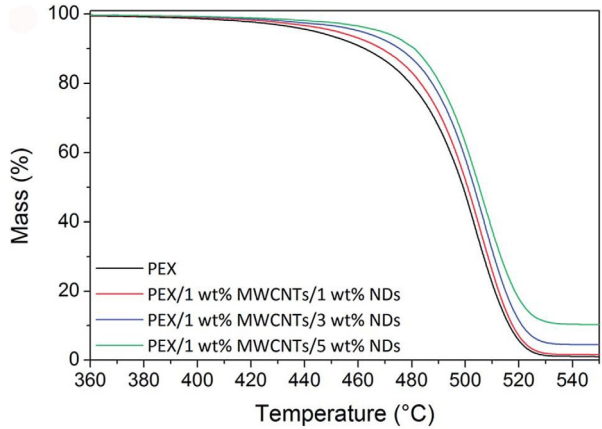

FIG. 11.22 Mass loss curves of PEX composites with 1 wt% MWCNTs/1–5 wt% NDs. *Reprinted from E. Roumeli, et al., Understanding the mechanical and thermal property reinforcement of crosslinked polyethylene by nanodiamonds and carbon nanotubes, RSC Adv. 4(85) (2014) 45522–45534 with permission from The Royal Society of Chemistry.*

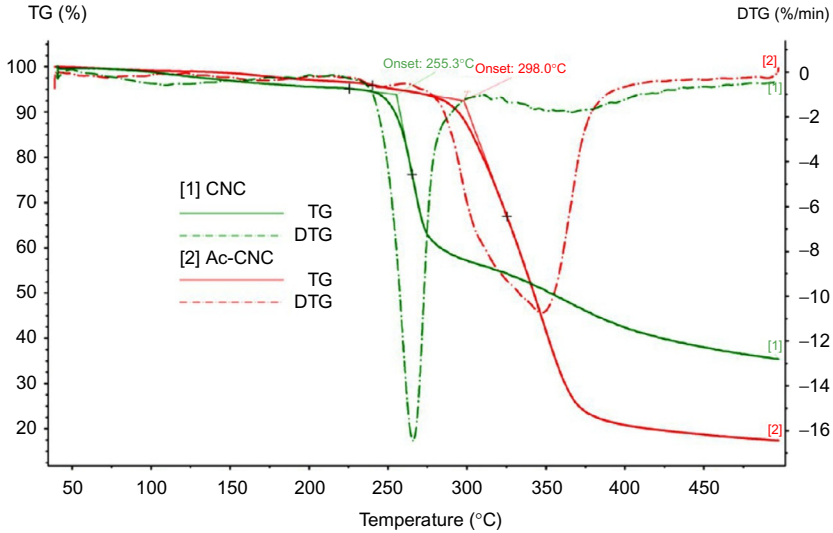

FIG. 11.23 TGA and DTG of CNC and Ac-CNC. *Reprinted from E. Abraham, et al., Highly modified cellulose nanocrystals and formation of epoxy-nanocrystalline cellulose (CNC) nanocomposites, ACS Appl. Mater. Interfaces 8(41) (2016) 28086–28095 with permission from American Chemical Society.*

Thermal analysis of Ac-CNC show a wide range of single degradation steps in the temperature range of 290–400°C and much higher thermal stability than CNC with a decomposition onset at 298°C, while for CNC it was at 255°C. Authors suggested that the long pendant alkyl groups, prevented early thermal degradation of the Ac-CNC cellulose structure.

Carvalho et al. [111] studied the radical trapping flame retardant mechanism of PMMA-clay nanocomposites as frequently claimed to be responsible for improving the thermal stability of polymers. Three natural MMT clays with different atomic ratio of structural Fe ions: Arizona (0.32 at.% of Fe), Wyoming (1.02 at.% of Fe), and Nontronite (8.10 at.% of Fe) were incorporated into PMMA. TG curves of the 6 wt% loaded PMMA-MMT nanocomposites are displayed in Fig. 11.24.

The barrier effects were expected to be similar for all nanocomposites containing the same clay loading—the addition of clays significantly shifts by about 100°C the onset of the mass loss, characterizing a dominant diffusion barrier effect. Radical trapping effect caused by iron was also postulated.

Thermal stability of PEO confined in GO was investigated by Barroso-Bujans et al. [112]. They found that PEO/GO intercalation compounds' decomposition starts at 50°C lower than that of pristine GO, and at 160°C lower than neat PEO, as observed in the TG profiles presented in Fig. 11.25.

The mass loss and DTG data for PEO/GO show that the thermal decomposition of this compound occurs in two main steps, at 195°C and 287°C,

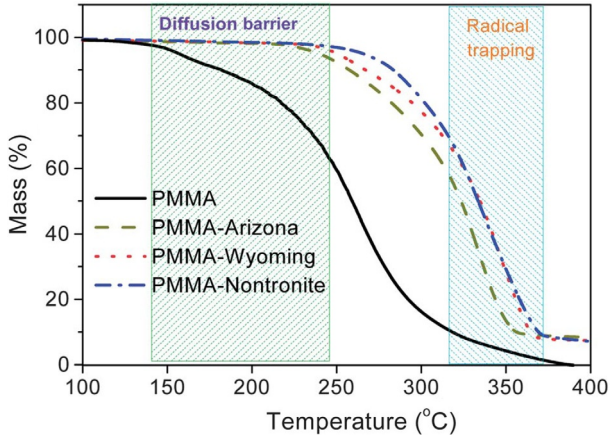

FIG. 11.24 Thermogravimetric curves of pristine PMMA and PMMA-MMT nanocomposite containing 6 wt% of clay (Arizona 0.32 at.% of Fe, Wyoming 1.02 at% of Fe, and Nontronite 8.10 at.% of Fe). *Reprinted from H.W.P. Carvalho, et al., Polymer-clay nanocomposites thermal stability: experimental evidence of the radical trapping effect, RSC Adv. 3(45) (2013) 22830–22833 with permission from The Royal Society of Chemistry.*

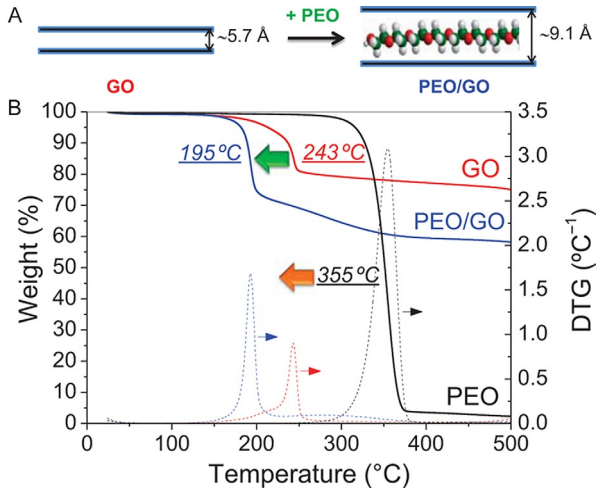

FIG. 11.25 (A) Sketch of PEO intercalation into GO interlayer causing an expansion from ca. 5.7 to 9.1 Å. (B) TGA and DTG showing the decrease in decomposition temperature of pristine GO and neat PEO when PEO is intercalated into GO interlayer (PEO/GO). The composition is 24 wt% of PEO in PEO/GO, which corresponds to the maximum uptake of PEO in GO. T_p of PEO/GO is 50°C lower than that of pristine GO and 160°C lower than neat PEO. Heating rate: 1°C/min, atmosphere: nitrogen. *Reprinted from F. Barroso-Bujans, et al., Thermal stability of polymers confined in graphite oxide, Macromolecules 46(5) (2013) 1890–1898 with permission from American Chemical Society.*

whereas that for neat GO and PEO occurs at 243°C and 355°C, respectively. Remarkably, this behavior was independent of the chain length of PEO and of the degree of GO oxidation.

11.4.5.2 Thermal Degradation Kinetics

By using TG it was found that HAp nanoparticles lead to a significant decrease of POM thermal stability [113,114]. Based on TG results obtained at different heating rates, kinetic parameters of POM and POM in POM/HAp nanocomposites degradation were calculated using isoconversional Friedman and Ozawa-Flynn-Wall methods, and then multiple nonlinear regression method. Degradation of neat POM copolymers proceeds on one main stage, the initial reaction is autocatalytically activated and it depends on the polymer mass-average molar mass. For POM/HAp nanocomposites with higher average POM molar mass, parallel autocatalytic and phase-boundary reaction model were found as the best fit. If POM with the lowest molar mass was utilized, additional parallel diffusion-controlled reaction was found to be a rate-controlling mechanism [114].

11.4.6 Thermoanalytical Methods (TG/MS, TG/FTIR)

From conventional TG alone, no chemical information about the gases evolved on heating can be obtained. To increase the capability of TG for materials characterization other techniques are coupled with thermogravimetry in order to identify either the residue or the products evolved during the experiment [115]. The most popular is coupling TG with infrared (IR) or mass spectrometry (MS) techniques, which enable to identify the compounds evolved and to determine the temperature range over which they are released [116]. Both simultaneous and sequential techniques have been developed for identification of these gases and volatiles and they are known as evolved gas analysis methods [117–121]. According to the IUPAC Compendium of Chemical Terminology the evolved gas analysis is a "technique in which the nature and/or amount of volatile product(s) released by a substance subjected to a controlled temperature program is (are) determined" [122].

An example of application of thermoanalytical techniques for investigation of PNCs is related to the assessment of the influence of nanohydroxyapatite (HAp) on the thermal stability and degradation mechanism of POM [114,123]. During melt processing of POM nanocomposites it was observed that the introduction of higher amounts of HAp causes decomposition of POM matrix; to identify the degradation products, TG-FTIR (Fig. 11.26) and TG-MS were applied.

On FTIR spectra, several absorption bands were detected: at ca. 1033 cm^{-1} (C═O in aldehydes or carbon monoxide), 1104, 1121, 1162 cm^{-1} (νC—O in ethers and esters) 1209 cm^{-1} (νC—O for acids), 1745 cm^{-1} (νC═O in aldehydes), 1755 cm^{-1} (νC═O in esters or acids), and at 2800 cm^{-1} (CH_2 in aldehydes) [124]. Results suggested that the main degradation products of pristine h-POM and h-POM/1% HAp composite are formaldehyde resulting from

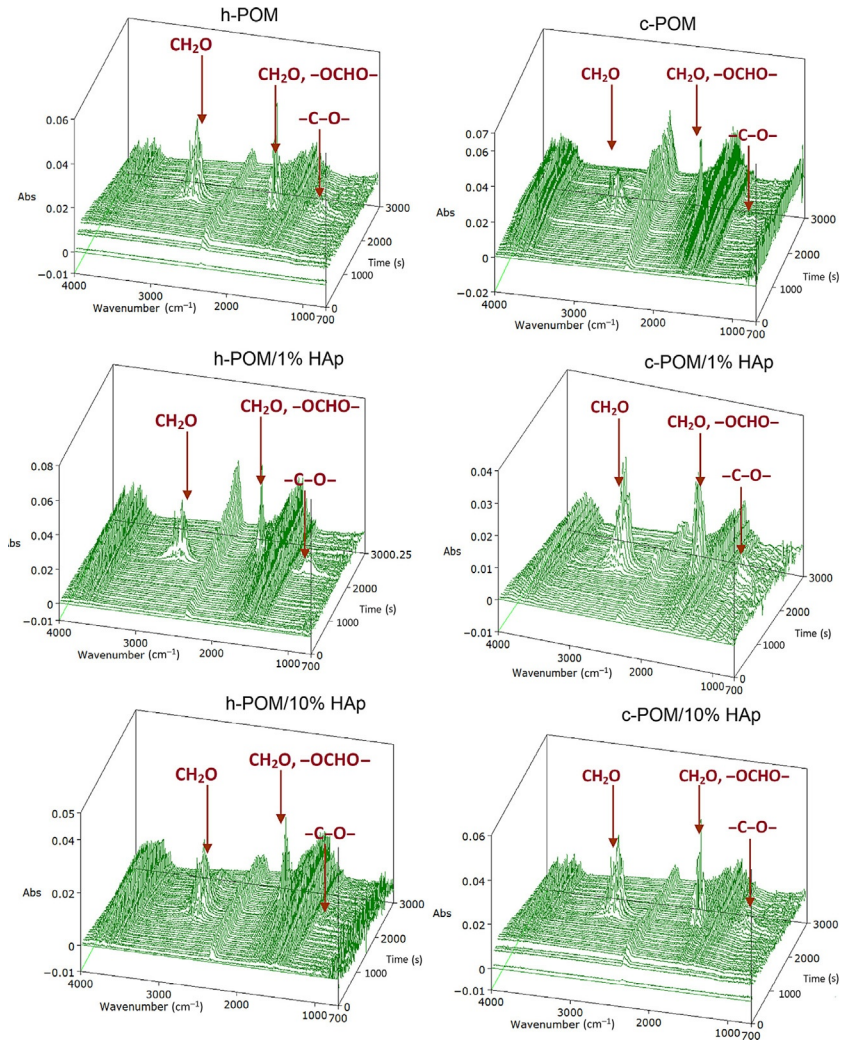

FIG. 11.26 Stacked plot of IR spectra of volatile products evolved during the thermal degradation of POM homopolymer and copolymer and their nanocomposites with HAp. *Reprinted from K. Pielichowska, Thermooxidative degradation of polyoxymethylene homo- and copolymer nanocomposites with hydroxyapatite: kinetic and thermoanalytical study, Thermochim. Acta (2015), https://doi.org/10.1016/j.tca.2014.11.016 with permission from Elsevier.*

depolymerization reaction of chain ends and random chain scission of oxymethylene chains. Formic acid, acetic acid, methanol (or ethanol), and methyl formate are also formed, but in smaller amounts. For nanocomposite h-POM/10% HAp peaks at 1033 cm^{-1} (C═O in aldehydes or carbon monoxide), 1104, 1121, 1162 cm^{-1} (νC—O in ethers and esters), and 1209 cm^{-1}

(νC—O for acids) are very small or were not detected, and the main degradation product was formaldehyde. FTIR results confirmed TG-MS and kinetic analysis data and also proved that formaldehyde formation during POM degradation is preferred and probably catalyzed by HAp nanoparticles.

TG-MS was applied to investigate the differences in thermal degradation of POM with various mass-average molar mass and its nanocomposites (Fig. 11.27).

During the thermal degradation of POM fragmentation ions, *m/z* 17 (—OH), *m/z* 18 (water), *m/z* 29 (fragment of $H_2C{=}O$ and other components), *m/z* 30 (formaldehyde), *m/z* 31 (fragment of CH_3—OH and trioxane), and *m/z* 44 (carbon dioxide), were detected. The largest intensity of formaldehyde evolution was observed for POM/HAp nanocomposites, in particular for POM with lower average molar mass, whereby the highest amount of water (*m/z* 18), methanol (*m/z* 31), and carbon dioxide (*m/z* 44) were formed for neat POM. It was postulated that addition of HAp causes a decrease in the amount of degradation products other than formaldehyde, compared to neat POM; additionally, the amount of released formaldehyde depends on the POM molar mass.

Cervantes et al. [125] applied TG-FTIR to study degradation mechanism of segmented polyurethane (sPU)/clay nanocomposites. The results proved that the thermal degradation of unfilled sPU and the 4, 6, and 10 wt% clay containing nanocomposites (hand-mixed) occurred in two main stages: (a) the degradation of hard segments, and (b) the degradation of soft segments. Thermal stability of the investigated nanocomposites was not improved by increasing nanoclay concentration except for sPU/organically modified MMTs nanocomposites where a 40°C increase in thermal stability was reported. For nanocomposites prepared by an in situ polymerization, higher thermal stability than for corresponding hand-mixed nanocomposites, was observed. In addition, during the second degradation stage these nanocomposites displayed the presence of carbon dioxide in the evolved gases, which was not observed in the hand-mixed nanocomposites (Fig. 11.28).

Authors postulated that the presence of clay in the nanocomposites has a significant effect on the thermal degradation pathways—the metallic species within the aluminosilicate potentially catalyze reactions between carbonaceous residue and oxygen in the layered structure of the MMT yielding CO_2 [126]. This hypothesis is supported by the findings of Takeichi et al. [127] who suggested that the layered silicates make the path longer for escaping the thermally decomposed volatiles (barrier effect), but some amounts of the thermally decomposed volatiles are captured by OMMT.

Degradation process of PS and a PS-clay composites was studied using pyrolysis-GC-MS and TG-FTIR methods by Vyazovkin et al. [128]. The results showed that the degradation mechanism of the PS-clay composite differs from that of neat PS with high yield of α-methylstyrene indicating intensification of intermolecular radical transfer reactions for nanocomposite materials.

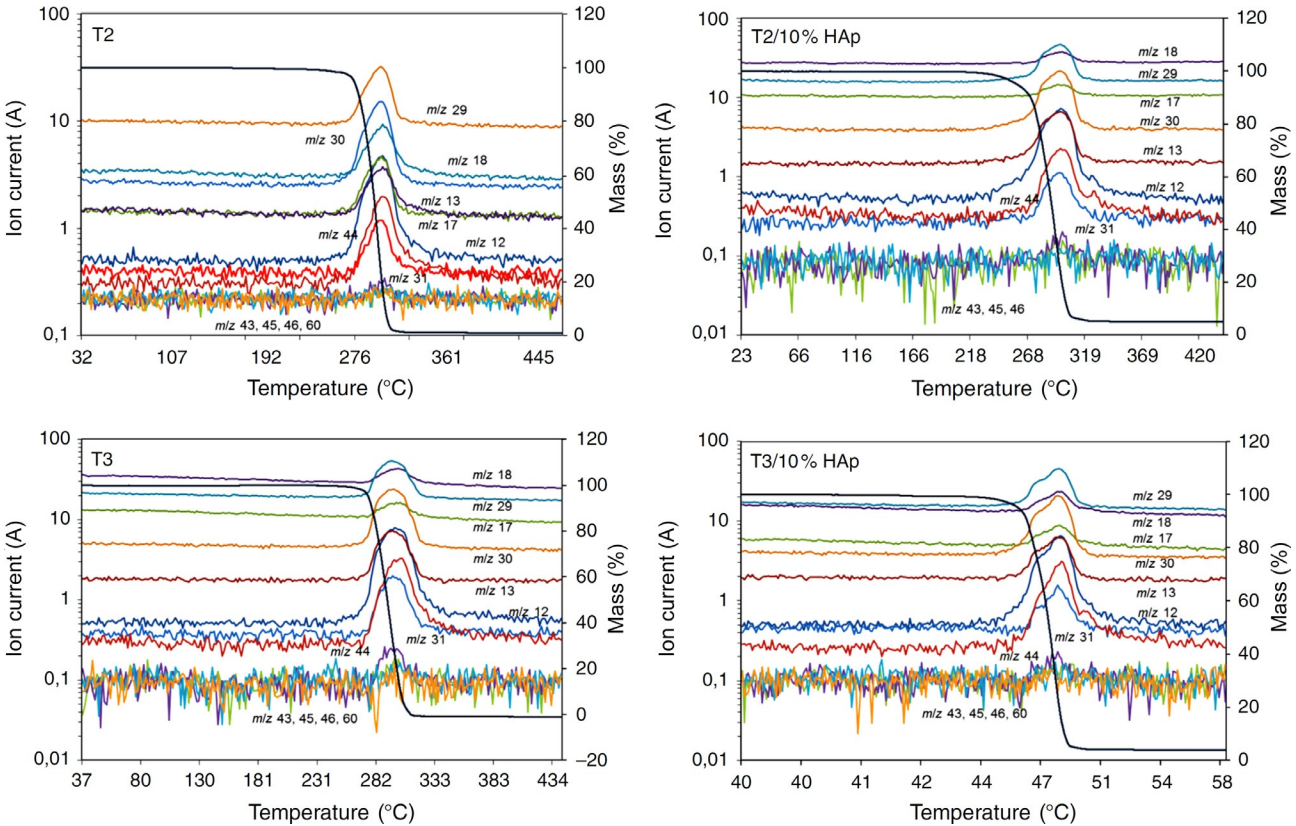

FIG. 11.27 Intensity of evolution of selected volatile products formed during the thermal degradation of POM and POM/HAp nanocomposites. *Reprinted from K. Pielichowska, The influence of polyoxymethylene molar mass on the oxidative thermal degradation of its nanocomposites with hydroxyapatite, J. Therm. Anal. Calorim. 124(2) (2016) 751–765 with permission from Springer.*

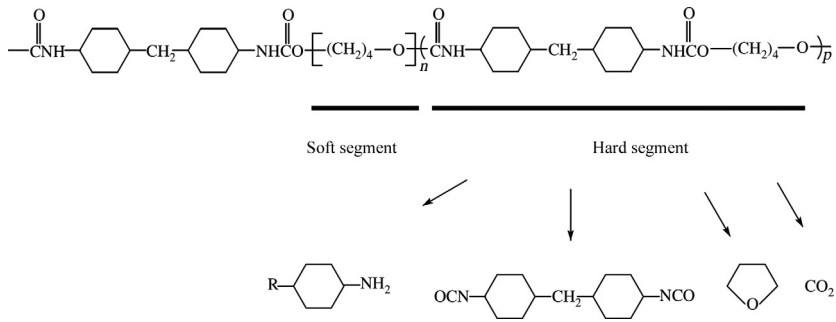

FIG. 11.28 Suggested mechanism of thermal degradation of sPU/Cloisite 30B nanocomposite prepared by in situ polymerization. *Reprinted from J.M. Cervantes-Uc, et al., TGA/FTIR studies of segmented aliphatic polyurethanes and their nanocomposites prepared with commercial montmorillonites, Polym. Degrad. Stab. 94(10) (2009) 1666–1677 with permission from Elsevier.*

11.4.7 DMA and TMA

DMA and TMA are high-efficient techniques for the characterization of mechanical properties and allow detailed exploration of glass transitions and relaxations or other secondary transitions in PNCs.

Zha et al. [129] investigated EP-based nanocomposites using DMA method. The typical DMA thermograms of neat EP and EP/TiO_2/MMT nanocomposites are presented in Fig. 11.29.

Authors observed that the storage modulus (E') for all nanocomposites went up to a higher value comparative to the unmodified EP and decreased with temperature increase, but retained a higher stiffness than the EP at the temperature above 150°C. The increase in E' was explained as a result of the full exfoliation of MMT layers in nanocomposites—exfoliated MMT sheet with surrounding TiO_2 nanoparticles was like extremely large and rigid cross-linking plane, which was equivalent to increase the amount of cross-links for the epoxy matrix and led to increased cross-linking density and stiffening effect on the epoxy matrix. With an increase of nanofillers content, the T_g peak of EP/TiO_2/MMT slightly shifts to the higher values compared with the unmodified EP. Increased cross-linking in nanocomposites leads to the confinement and the decline in the mobile range of molecule segments of polymer chains.

Pihan et al. [130] reported on mechanical properties and glass-transition temperature of a nanocomposite material consisting of swellable silsesquioxanes NPs with grafted poly(ethyl methacrylate) (PEMA) brushes and PEMA matrices with varying molecular weight, investigated by DMA method. Unstable dispersions of the matrix with high molecular weight due to incompatibility between polymer-grafted-nanoparticles and homopolymer matrices were found, and for these unstable dispersions, authors observed a decreased glass-transition temperature along with a decreased plateau modulus, which suggest the formation of a liquid-like layer at the brush-matrix interface.

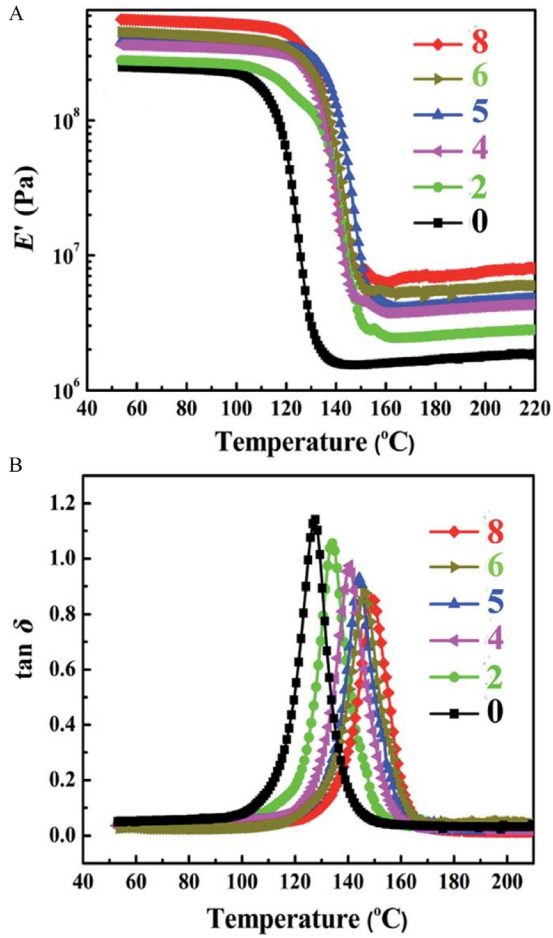

FIG. 11.29 Storage moduli (A) and tan δ curves (B) of neat EP and reinforced nanocomposites. *Reprinted from R. Zha, et al., Double dimensionally ordered nanostructures: toward a multifunctional reinforcing nanohybrid for epoxy resin, RSC Adv. 7(2) (2017) 1177–1190.*

Shi et al. [131] studied DMA three-dimensionally nanoporous cellulose gels (NCG) prepared from aqueous alkali hydroxide/urea solution. They obtained poly(MMA/BMA)/NCG, poly(MMA/BA)/NCG nanocomposites with a volume fraction of NCG from 15% to 78%. DMA results show a considerable increase of the tensile storage modulus E' above the glass-transition temperature for nanocomposites containing 15% (v/v) NCG—this large reinforcement effect was explained by the percolation model.

Glass transition and reinforcement mechanism in PLS nanocomposites were investigated by Zhang and Loo using DMA method [132]. They revealed that the type of polymer-nanofiller interaction strongly influences

the amount and modulus of the constrained region in nanocomposites, and both of the latter contribute to the enhancement in the storage modulus. Moreover, the mechanical property and reinforcement effect of the constrained region have also been found to be temperature-dependent. Authors concluded that DMA is deemed to be a suitable technique for obtaining pertinent information for the constrained volume. For instance, using Eq. (11.6) and the DMA data it is possible to determine the value of the storage modulus of the constrained region, E'_c at any temperature for each amorphous polymer/organoclay system:

$$\frac{E'_n}{E'_m} = \left(\frac{E'_c}{E'_m} - 1\right)C + 1 \tag{11.15}$$

where E'_n, E'_m, and E'_c are the storage modulus of the nanocomposite, the polymer matrix (i.e., amorphous PA), and the constrained region, respectively, C is the volume fraction of the constrained region [132].

Based on DMA results it is possible to calculate of activation energy of glass transition [133].

The dynamics of the α-relaxation is supposed to follow Vogel-Fulcher-Tamman relationship [134]:

$$f = f_0 e^{-\frac{B}{T-T_0}} \tag{11.16}$$

where f_0, B, and T_0 are parameters to be determined. However, the frequency range of the DMA is rather limited for the determination of all three of these parameters, and so a pseudo-Arrhenius behavior should be assumed:

$$f = f_0 e^{-\frac{E_{act}}{kT}} \tag{11.17}$$

In order to determine pseudo-activation energy from a linear fit on the Arrhenius map, as is shown for POM/HAp nanocomposites [135], it was revealed that E_a were larger for POM/HAp nanocomposites compared to neat POM (Fig. 11.30).

A similar trend was observed by other authors for different PNCs. Hence, Wong et al. [136] reported the linear increase in the glass-transition temperature of PMMA/ZnO nanocomposites vs ZnO quantum dots weight content. It was assumed that the confinement effect between nanoparticles affects T_g as a polymer thin film, which is sandwiched between two substrates [39,137].

Glass temperature values of the polyimide nanocomposites with functionalized SiO_2 nanoparticles were determined by TMA in the work of Kim et al. [138]. It was observed that the glass temperature for the nanocomposites gradually declined from 381.3°C to 363.3°C with the SiO_2 content increase. This effect was attributed to the interface between the polymer and the nanoparticle—nanoparticle surfaces acted as plasticizers for the polyimide.

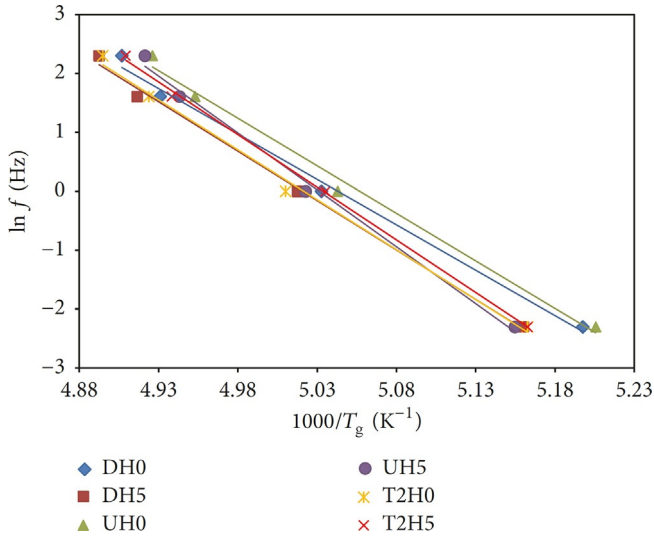

FIG. 11.30 Arrhenius frequency map of POM and POM/HAp nanocomposites calculated from DMA results. DMA points correspond to the γ peak at tanδ. *Reprinted from K. Pielichowska, et al., The influence of nanohydroxyapatite on the thermal, mechanical and tribological properties of polyoxymethylene nanocomposites, Int. J. Polym. Sci. (2017).*

11.4.8 Laser Flash Analysis (LFA)

A flash method for measuring the thermal diffusivity, heat capacity, and thermal conductivity was described for the first time in 1961 by Parker et al. [139]. They determined the thermal diffusivity from the shape of the temperature vs time curve at the rear surface, the heat capacity by the maximum temperature indicated by the thermocouple, and the thermal conductivity by the product of the heat capacity, thermal diffusivity, and the density. First they determined these values for metals: for copper, silver, iron, nickel, aluminum, tin, zinc, and some alloys at 22°C and 135°C and compared with previously reported values.

Generally, for homogeneous materials, thermal conductivity is connected with diffusivity using a fundamental equation:

$$\lambda = \alpha \cdot \rho \cdot C_p \tag{11.18}$$

where λ is thermal conductivity ($W\,m^{-1}\,K^{-1}$), α thermal diffusivity ($m^2\,s^{-1}$), ρ is density ($kg\,m^{-3}$), and C_p is specific heat capacity ($J\,kg^{-1}\,K^{-1}$) [140].

An example of application of flash method to determine thermal conductivity of PNCs was described by Choi et al. in work [141] where they studied polyamid6.6/nanodiamond (PA66/ND) systems. On the basis of thermal diffusivity measurements thermal conductivity was calculated (Table 11.2).

TABLE 11.2 Thermal Conductivities of the PA66 Composites as Nanodiamond Contents

	NDs (wt%)	Thermal Diffusivity (mm^2/s)	Specific Heat Capacity (J/(g K))	Thermal Conductivity (W/(m K))
Pristine ND	0	0.163 ± 0.010	1.667 ± 0.058	0.337 ± 0.032
	1	0.166 ± 0.011	1.759 ± 0.108	0.362 ± 0.046
	2	0.161 ± 0.009	1.851 ± 0.095	0.369 ± 0.039
	3	0.155 ± 0.001	1.943 ± 0.067	0.373 ± 0.015
PA66-g-sND	1	0.161 ± 0.002	1.773 ± 0.079	0.354 ± 0.020
	2	0.160 ± 0.004	1.879 ± 0.161	0.370 ± 0.040
	3	0.157 ± 0.001	1.985 ± 0.123	0.386 ± 0.026

Reprinted from E.-Y. Choi, et al., Reinforcement of nylon 6,6/nylon 6,6 grafted nanodiamond composites by in situ reactive extrusion, Sci. Rep. 6 (2016) 37010.

Thermal diffusivity of PA66 and ND composites did not show significant difference between PA66 and ND-incorporated PA66, while the thermal diffusivity of thePA66/ND composites decreases with addition of NDs. It has been concluded that the enhanced thermal conductivity of the ND-containing PA66 is contributed by the specific heat capacity, rather than the thermal diffusivity, and it was speculated that dispersion, adhesion, and interaction of the nanodiamond in the PA66 matrix might determine the final thermal conductivity [141].

In another work Roumeli et al. [109] studied the mechanical and thermal properties of reinforcement of silane-cross-linked PE nanocomposites with small amounts of MWCNTs and NDs. Authors found that two investigated nanofillers contribute differently to the observed thermal conductivity increase—MWCNTs significantly enhance the C_p of the composites and also cause a modest increase in their thermal diffusivity, while NDs only enhance the C_p resulting in a slightly more significant final conductivity increase.

Fluorinated-MWNTs/epoxy nanocomposites processed with a magnetic field have been studied by Abdalla et al. [142]. Nanocomposites were prepared by dispersing the F-MWCNTs in the EP and then cured under an applied magnetic field to partially align MWCNTs dispersed in an EP. The highest increase of thermal diffusivity and thermal conductivity of 69.2% and 107.1% from 0.13 to 0.22 mm^2/s and 0.14 to 0.29 W/(m K), respectively, was recorded for the composite reinforced with the randomly oriented F-MWCNT, while the nanocomposites produced with the F-MWCNT perpendicular to the laser pulse, exhibited a lower increase of 30.8% and 71.4% from 0.13 to 0.17 mm^2/s and 0.14 to 0.24 W/(m K) for thermal diffusivity and conductivity, respectively.

11.4.9 DETA

The term DETA is connected to a group of techniques that measure changes in different physical properties of a polar material, such as polarization, permittivity, and conductivity, with temperature and/or frequency [143].

Since the mid-1970s, DETA has been recognized as a powerful thermal analysis method for investigating condensed- and soft-matter dynamics. This technique was intensively used in the dielectric characterization of ion-conducting solids, mesophases (liquid crystals, etc.), biological systems, colloids, emulsions, and particularly polymers and related composites or nanocomposites [144].

Hence, Al-Hartomy et al. [145] investigated the influence of fullerenes on the vulcanization characteristics of natural rubber and dielectric properties of nanocomposites and siloxane rubber-based composites filled with carbon black [146]. The dielectric properties were measured using DETA to characterize the relaxation behavior of the obtained materials. The frequency dependence of dielectric permittivity at different degree of fullerene filling ranged from 0 to 1.5 phr at 30°C and is presented in Fig. 11.31.

Values of dielectric permittivity ε' for filler loadings 0.5 and 1.0 phr samples are very similar but when the filler loading increase up to 1.5 phr an increase of dielectric permittivity was observed. Dielectric permittivity decreases with an increase of frequency—this effect was explained by rubber macromolecules polarization at higher frequency.

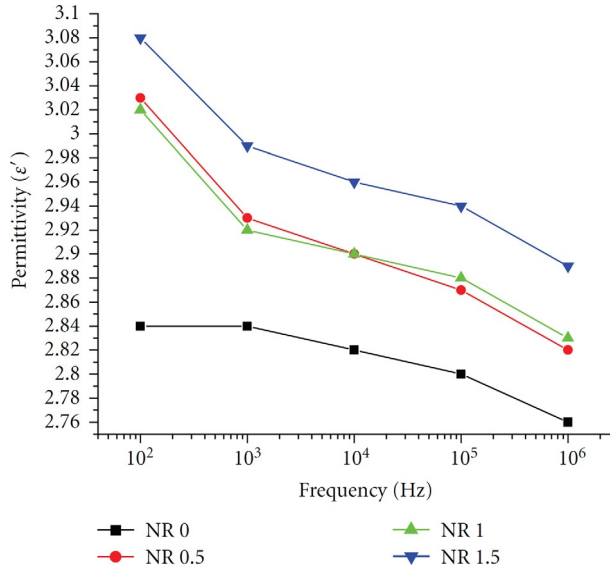

FIG. 11.31 Frequency dependence of dielectric permittivity at different degree of fullerene filling, at 30°C. *Reprinted from O.A. Al-Hartomy, et al., Properties of natural rubber-based composites containing fullerene, Int. J. Polym. Sci. 2012 (2012) 8.*

Rao and Pochan [147] studied copolymer latex ($PBSMaSO_3$) with MMT clay using DMA and DETA to study the chain mobility. By measuring the induced polarization, DETA can quantify the amount of material participating in the glass transition because the height of the imaginary part of the dielectric constant (ε'') is proportional to the number of the mobile dipoles during the glass transition [147,148]. Thus, the decrease in the ε'' characterizes the immobilization of the polymer chains as it was observed in the system under investigation (Fig. 11.32).

Application of DETA for the real-time assessment of the dispersion of carbon nanotubes in epoxy was proposed by Bekas et al. [149] who performed process monitoring using DETA to measure the evolution of the impedance of the mixture during ultrasonication. Based on DEA results, the dispersion process was divided into few stages. In the initial stage of ca. 10 min CNTs approach the resin molecules and each entity keeps its individual properties in large scale. This stage was accompanied by the temperature increase and a decrease in both real and imaginary parts of the impedance. In the next stage, corresponding to 10–80 min the viscosity of the mixture increased due to the deagglomeration of the CNTs and a significant increase in real and imaginary parts is observed. In the last stage, corresponding to 80–120 min, the dipoles show negligible contribution to polarization, while the ions appear trapped in the high viscous medium. Both real and imaginary parts of the impedance reach their final values while the resistance of the CNT contribution is really low and the inductance reaches high values. After the dispersion process, the acceptable dispersion quality was achieved [149].

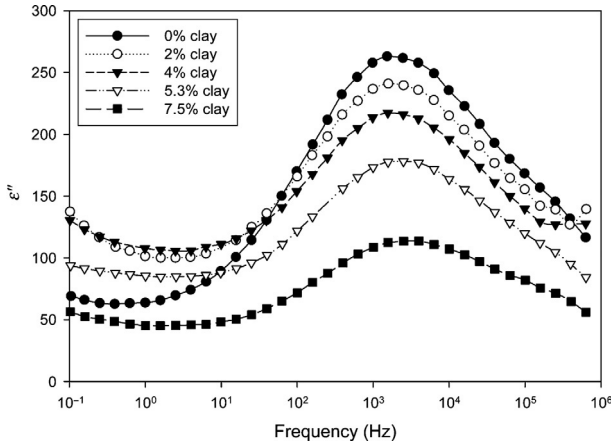

FIG. 11.32 Chain constraint in polymer clay nanocomposites studied by DETA: trace of ε'' vs frequency as measured by DETA at room temperature (the percentage in legends are volume percentage). *Reprinted from Y. Rao, J.M. Pochan, Mechanics of polymer-clay nanocomposites, Macromolecules 40(2) (2007) 290–296 with permission from American Chemical Society.*

11.5 CONCLUSIONS

PNCs containing nanosize fillers, although investigated since more than two decades, are still the subject of numerous research programs at both academia and industry as they exhibit different physical, chemical, and biological properties and functions than the same material in microscale. An additional advantage is that, in contrast to conventional polymer composites with high loadings (even up to 60 vol%) of microsized filler, PNCs contain usually low loadings (less than 5 vol%) of nanofillers. Incorporation of nanosize additives into polymer matrix can substantially change its glass transition, melting, and crystallization behavior. It is important to follow the changes in the dynamics of the interphase region between matrix and polymers bound on nanoparticles in order to understand the mechanical and rheological properties of PNCs. Dynamics of polymer chains, controlled by entanglements that are topological constraints exerted by the neighboring chains, is considerably influenced by the presence of nanoparticles. Processes like diffusion of the nanostructures in the host polymer, which facilitates polymer chain relaxation by constraint release, have been considered to influence glass-transition temperature of polymer matrix. Depending on the shape, size, amount, chemical structure, and the polymer radius of gyration, the addition of nanoparticles can enhance or slow down polymer chain dynamics. Thermal analysis methods are widely applied to characterize the thermal properties and behavior of polymer-based nanocomposites and to study effects associated with the presence of nanoparticles dispersed in polymer matrix. Numerous works have been devoted to investigate the influence of nanoparticles on phase transitions and degradation processes of nanostructured polymeric materials. For instance, changes in crystallization behavior, studied by DSC technique, have been explained by effective nucleation at low nanoadditive loadings, but at higher loadings hindering of the crystallization process by disturbing growing fronts occurred. TG data gave a deeper insight into thermal decomposition processes in PNCs and help to formulate the mechanisms responsible for higher thermal stability, such as barrier mechanism for clay-containing systems. New methods, such as TMDSC, offer the possibilities to study overlapping phenomena with improved resolution and enhanced sensitivity, whereby DFSC is an attractive tool to study kinetics, thermodynamics, and phase transitions of materials that are in the state far from thermodynamic equilibrium.

ACKNOWLEDGMENTS

Authors are grateful to the Polish National Science Centre for financial support of projects under the Contracts No. 2015/19/B/ST8/01060 (Krzysztof Pielichowski) and 2016/21/B/ST8/00449 (Kinga Pielichowska).

REFERENCES

[1] A. Leszczyńska, et al., Polymer/montmorillonite nanocomposites with improved thermal properties: part I. Factors influencing thermal stability and mechanisms of thermal stability improvement, Thermochim. Acta 453 (2) (2007) 75–96.

[2] G. Keledi, J. Hari, B. Pukanszky, Polymer nanocomposites: structure, interaction, and functionality, Nanoscale 4 (6) (2012) 1919–1938.

[3] A. Leszczynska, K. Pielichowski, Application of thermal analysis methods for characterization of polymer/montmorillonite nanocomposites, J. Therm. Anal. Calorim. 93 (3) (2008) 677–687.

[4] D.R. Paul, L.M. Robeson, Polymer nanotechnology: nanocomposites, Polymer 49 (15) (2008) 3187–3204.

[5] E.T. Thostenson, C. Li, T.-W. Chou, Nanocomposites in context, Compos. Sci. Technol. 65 (3–4) (2005) 491–516.

[6] J. Koo, 1—Introduction to nanotechnology, in: Fundamentals, Properties, and Applications of Polymer Nanocomposites, Cambridge University Press, New York, USA, 2017.

[7] J. Jancar, et al., Current issues in research on structure–property relationships in polymer nanocomposites, Polymer 51 (15) (2010) 3321–3343.

[8] L.S. Schadler, L.C. Brinson, W.G. Sawyer, Polymer nanocomposites: a small part of the story, JOM 59 (3) (2007) 53–60.

[9] F. Hussain, et al., Review article: polymer-matrix nanocomposites, processing, manufacturing, and application: an overview, J. Compos. Mater. 40 (17) (2006) 1511–1575.

[10] J. Choi, et al., Universal scaling of polymer diffusion in nanocomposites, ACS Macro Lett. 2 (6) (2013) 485–490.

[11] D. Kim, et al., Polymer nanocomposites: polymer and particle dynamics, Soft Matter 8 (42) (2012) 10813–10818.

[12] T. Uemura, et al., Unveiling thermal transitions of polymers in subnanometre pores, Nat. Commun. 1 (2010) 83.

[13] E.P.Giannelis, R. Krishnamoorti, E. Manias, Polymer-silicate nanocomposites: model systems for confined polymers and polymer brushes, in: S. Granick et al. (Ed.), Polymers in Confined Environments, Springer Berlin Heidelberg, Berlin, Heidelberg, 1999, pp. 107–147.

[14] J. Ding, P. Maitra, S.L. Wunder, Characterization of the interaction of poly(ethylene oxide) with nanosize fumed silica: surface effects on crystallization, J. Polym. Sci. B: Polym. Phys. 41 (17) (2003) 1978–1993.

[15] G.J. Papakonstantopoulos, et al., Local mechanical properties of polymeric nanocomposites, Phys. Rev. E 72 (3) (2005). 031801.

[16] W. Zhao, et al., Interfacial effect on confined crystallization of poly(ethylene oxide)/silica composites, J. Polym. Sci. B: Polym. Phys. 54 (3) (2016) 414–423.

[17] C.-C. Lin, et al., Do attractive polymer–nanoparticle interactions retard polymer diffusion in nanocomposites? Macromolecules 46 (11) (2013) 4502–4509.

[18] S. Gam, et al., Polymer diffusion in a polymer nanocomposite: effect of nanoparticle size and polydispersity, Soft Matter 8 (24) (2012) 6512–6520.

[19] S. Gam, et al., Macromolecular diffusion in a crowded polymer nanocomposite, Macromolecules 44 (9) (2011) 3494–3501.

[20] M. Rubinstein, R.H. Colby, Polymer Physics, OUP, Oxford, 2003.

[21] M. Doi, S.F. Edwards, The Theory of Polymer Dynamics, International Series of Monographs on Physics, Clarendon Press, Oxford, 1988.

[22] T.C.B. McLeish, Tube theory of entangled polymer dynamics, Adv. Phys. 51 (6) (2002) 1379–1527.
[23] A. Karatrantos, et al., Entanglements in polymer nanocomposites containing spherical nanoparticles, Soft Matter 12 (9) (2016) 2567–2574.
[24] P.E. Rouse, A theory of the linear viscoelastic properties of dilute solutions of coiling polymers, J. Chem. Phys. 21 (7) (1953) 1272–1280.
[25] S.F. Edwards, The statistical mechanics of polymerized material, Proc. Phys. Soc. 92 (1) (1967) 9.
[26] P.G. de Gennes, Reptation of a polymer chain in the presence of fixed obstacles, J. Chem. Phys. 55 (2) (1971) 572–579.
[27] M. Doi, S.F.Edwards, Dynamics of concentrated polymer systems. Part 1. Brownian motion in the equilibrium state, J. Chem. Soc., Faraday Trans. 2 74 (1978) 1789–1801.
[28] M. Doi, S.F. Edwards, Dynamics of concentrated polymer systems. Part 2. Molecular motion under flow, J. Chem. Soc., Faraday Trans. 2 74 (1978) 1802–1817.
[29] M. Doi, S.F. Edwards, Dynamics of concentrated polymer systems. Part 3. The constitutive equation, J. Chem. Soc., Faraday Trans. 2 74 (1978) 1818–1832.
[30] M. Doi, S.F. Edwards, Dynamics of concentrated polymer systems. Part 4. Rheological properties, J. Chem. Soc., Faraday Trans. 2 75 (1979) 38–54.
[31] T.A. Kavassalis, J. Noolandi, A new theory of entanglements and dynamics in dense polymer systems, Macromolecules 21 (9) (1988) 2869–2879.
[32] A.S. Sarvestani, C.R. Picu, A frictional molecular model for the viscoelasticity of entangled polymer nanocomposites, Rheol. Acta 45 (2) (2005) 132.
[33] R. Mangal, S. Srivastava, L.A. Archer, Phase stability and dynamics of entangled polymer-nanoparticle composites, Nat. Commun. 6:7198 (2015) 1–9.
[34] E. Senses, A. Faraone, P. Akcora, Microscopic chain motion in polymer nanocomposites with dynamically asymmetric interphases, Sci. Rep. 6 (2016) 29326.
[35] J.L. Keddie, R.A.L. Jones, R.A. Cory, Size-dependent depression of the glass transition temperature in polymer films, Europhys. Lett. 27 (1) (1994) 59.
[36] J.L. Keddie, R.A.L. Jones, R.A. Cory, Interface and surface effects on the glass-transition temperature in thin polymer films, Faraday Discuss. 98 (1994) 219–230.
[37] C. Zhang, Y. Guo, R.D. Priestley, Confined glassy properties of polymer nanoparticles, J. Polym. Sci. B: Polym. Phys. 51 (7) (2013) 574–586.
[38] F.W. Starr, et al., Bound layers "cloak" nanoparticles in strongly interacting polymer nanocomposites, ACS Nano 10 (12) (2016) 10960–10965.
[39] A. Bansal, et al., Quantitative equivalence between polymer nanocomposites and thin polymer films, Nat. Mater. 4 (9) (2005) 693–698.
[40] C.Y. Li, Polymer single crystal meets nanoparticles, J. Polym. Sci. B: Polym. Phys. 47 (24) (2009) 2436–2440.
[41] K. Pielichowska, et al., A study on the melting and crystallization of polyoxymethylene-copolymer/hydroxyapatite nanocomposites, Polym. Adv. Technol. 24 (3) (2013) 318–330.
[42] K. Jiang, et al., Solid–solid phase transition of n-alkanes in multiple nanoscale confinement, J. Phys. Chem. B 114 (3) (2010) 1388–1392.
[43] N. Ning, et al., Realizing the enhancement of interfacial interaction in semicrystalline polymer/filler composites via interfacial crystallization, Prog. Polym. Sci. 37 (10) (2012) 1425–1455.
[44] S. Yang, et al., Graphene oxide induced isotactic polypropylene crystallization: role of structural reduction, RSC Adv. 6 (28) (2016) 23930–23941.

[45] C. Chen, et al., Unexpected observation of highly thermostable transcrystallinity of poly(lactic acid) induced by aligned carbon nanotubes, Eur. Polym. J. 63 (2015) 177–185.
[46] S. Zhang, et al., Polymer transcrystallinity induced by carbon nanotubes, Polymer 49 (5) (2008) 1356–1364.
[47] C.Y. Li, et al., Nanohybrid shish-kebabs: periodically functionalized carbon nanotubes, Adv. Mater. 17 (9) (2005) 1198–1202.
[48] M. Ochoa, et al., Nanocellulose-PE-b-PEG copolymer nanohybrid shish-kebab structure via interfacial crystallization, Carbohydr. Polym. 159 (2017) 116–124.
[49] L. Zhang, T. Tao, C. Li, Formation of polymer/carbon nanotubes nano-hybrid shish–kebab via non-isothermal crystallization, Polymer 50 (15) (2009) 3835–3840.
[50] L. Li, et al., Carbon nanotube induced polymer crystallization: the formation of nanohybrid shish–kebabs, Polymer 50 (4) (2009) 953–965.
[51] C. Li, et al., Conformational regulation and crystalline manipulation of PLLA through a self-assembly nucleator, Biomacromolecules 18 (4) (2017) 1440–1448.
[52] N. Ning, et al., Largely enhanced crystallization of semi-crystalline polymer on the surface of glass fiber by using graphene oxide as a modifier, Polymer 54 (1) (2013) 303–309.
[53] N. Ning, et al., Interfacial enhancement by shish–calabash crystal structure in polypropylene/inorganic whisker composites, Polymer 50 (15) (2009) 3851–3856.
[54] C. Schick, Differential scanning calorimetry (DSC) of semicrystalline polymers, Anal. Bioanal. Chem. 395 (6) (2009) 1589.
[55] T.-C. Li, et al., Effect of clay addition on the morphology and thermal behavior of polyamide 6, J. Appl. Polym. Sci. 103 (2) (2007) 1191–1199.
[56] D. Wan, et al., Dependence of microstructures and melt behaviour of polypropylene/fullerene C60 nanocomposites on in situ interfacial reaction, Soft Matter 7 (11) (2011) 5290–5299.
[57] S. Yang, et al., Formation mechanism and morphology of β-transcrystallinity of polypropylene induced by two-dimensional layered interface, Macromolecules 48 (12) (2015) 3965–3973.
[58] J. Varga, β-modification of isotactic polypropylene: preparation, structure, processing, properties, and application, J. Macromol. Sci. B 41 (4–6) (2002) 1121–1171.
[59] K. Pielichowska, Polyoxymethylene-homopolymer/hydroxyapatite nanocomposites for biomedical applications, J. Appl. Polym. Sci. 123 (4) (2012) 2234–2243.
[60] K. Pielichowska, A. Szczygielska, E. Spasowka, Preparation and characterization of polyoxymethylene-copolymer/hydroxyapatite nanocomposites for long-term bone implants, Polym. Adv. Technol. 23 (8) (2012) 1141–1150.
[61] J. Mohanraj, et al., Physical and mechanical characterization of oriented polyoxymethylene produced by die-drawing and hydrostatic extrusion, Polymer 47 (16) (2006) 5897–5908.
[62] B. Wunderlich, Macromolecular Physics: Crystal Melting, Elsevier Science, New York, USA, 2013.
[63] X. Xu, et al., Comparison between cellulose nanocrystal and cellulose nanofibril reinforced poly(ethylene oxide) nanofibers and their novel shish-kebab-like crystalline structures, Macromolecules 47 (10) (2014) 3409–3416.
[64] X. Xu, et al., Preparation and properties of electrospun soy protein isolate/polyethylene oxide nanofiber membranes, ACS Appl. Mater. Interfaces 4 (8) (2012) 4331–4337.
[65] F. Shiravand, et al., Thermal analysis of polymer layered silicate nanocomposites, J. Therm. Anal. Calorim. 118 (2) (2014) 723–729.

[66] J.M. Hutchinson, The application of thermal analysis to the study of epoxy–clay nanocomposites, J. Therm. Anal. Calorim. 125 (2) (2016) 617–628.
[67] J.M. Hutchinson, F. Shiravand, Y. Calventus, Intra- and extra-gallery reactions in trifunctional epoxy polymer layered silicate nanocomposites, J. Appl. Polym. Sci. 128 (5) (2013) 2961–2970.
[68] J.H. Park, S.C. Jana, Mechanism of exfoliation of nanoclay particles in epoxy − clay nanocomposites, Macromolecules 36 (8) (2003) 2758–2768.
[69] I.-J. Chin, et al., On exfoliation of montmorillonite in epoxy, Polymer 42 (13) (2001) 5947–5952.
[69a] F. Shiravand, J.M. Hutchinson, Y. Calventus, Influence of the isothermal cure temperature on the nanostructure and thermal properties of an epoxy layered silicate nanocomposite, Polym. Eng. Sci. 54 (1) (2014) 51–58.
[70] A. Greco, R. Gennaro, M. Rizzo, Glass transition and cooperative rearranging regions in amorphous thermoplastic nanocomposites, Polym. Int. 61 (8) (2012) 1326–1333.
[71] M.J. Richardson, N.G. Savill, Derivation of accurate glass transition temperatures by differential scanning calorimetry, Polymer 16 (10) (1975) 753–757.
[72] J.M. Hutchinson, Determination of the glass transition temperature, J. Therm. Anal. Calorim. 98 (3) (2009) 579.
[73] A.Q. Tool, C.G. Eicitlin, Variations caused in the heating curves of glass by heat treatment, J. Am. Ceram. Soc. 14 (4) (1931) 276–308.
[74] O.S. Narayanaswamy, A model of structural relaxation in glass, J. Am. Ceram. Soc. 54 (10) (1971) 491–498.
[75] C.T. Moynihan, et al., Dependence of the fictive temperature of glass on cooling rate, J. Am. Ceram. Soc. 59 (1–2) (1976) 12–16.
[76] K. Pielichowska, et al., TOPEM DSC study of glass transition region of polyurethane cationomers, Thermochim. Acta 545 (2012) 187–193.
[77] L.D. Pye, et al., The Physics of Non-Crystalline Solids, Taylor & Francis, London, Washington DC, 1992.
[78] A.L. Flory, T. Ramanathan, L.C. Brinson, Physical aging of single wall carbon nanotube polymer nanocomposites: effect of functionalization of the nanotube on the enthalpy relaxation, Macromolecules 43 (9) (2010) 4247–4252.
[79] L.C.E. Struik, Physical Aging in Amorphous Polymers and Other Materials, Elsevier Scientific Publishing Company, Amsterdam, 1978.
[80] K. Chen, A.N. Baker, S. Vyazovkin, Formation and thermal behavior of polystyrene and polystyrene/clay gels, Macromol. Chem. Phys. 209 (23) (2008) 2367–2373.
[81] A. Saiter, H. Couderc, J. Grenet, Characterisationof structural relaxation phenomena in polymeric materials from thermal analysisinvestigations, J. Therm. Anal. Calorim. 88 (2) (2007) 483–488.
[82] C.A. Solunov, Cooperative molecular dynamics and strong/fragile behavior of polymers, Eur. Polym. J. 35 (8) (1999) 1543–1556.
[83] E. Donth, Characteristic length of the glass transition, J. Polym. Sci. B: Polym. Phys. 34 (17) (1996) 2881–2892.
[84] P. Klonos, P. Pissis, Effects of interfacial interactions and of crystallization on rigid amorphous fraction and molecular dynamics in polylactide/silica nanocomposites: a methodological approach, Polymer 112 (2017) 228–243.
[85] P. Klonos, et al., Glass transition and segmental dynamics in poly(l-lactic acid)/graphene oxide nanocomposites, Thermochim. Acta 617 (2015) 44–53.

[86] J.M. Hutchinson, S. Montserrat, The application of modulated differential scanning calorimetry to the glass transition of polymers. I. A single-parameter theoretical model and its predictions, Thermochim. Acta 286 (2) (1996) 263–296.
[87] M. Reading, A. Luget, R. Wilson, Modulated differential scanning calorimetry, Thermochim. Acta 238 (1994) 295–307.
[88] M. Reading, Modulated differential scanning calorimetry—a new way forward in materials characterisation, Trends Polym. Sci. 1 (1993) 248–253.
[89] S. Sauerbrunn, B. Crowe, M. Reading, Modulated differential scanning calorimetry, Am. Lab. 24 (1992) 44–47.
[90] A. Boller, C. Schick, B. Wunderlich, Modulated differential scanning calorimetry in the glass transition region, Thermochim. Acta 266 (1995) 97–111.
[91] J.E.K. Schawe, Principles for the interpretation of modulated temperature DSC measurements. Part 1. Glass transition, Thermochim. Acta 261 (1995) 183–194.
[92] J.E.K. Schawe, et al., Stochastic temperature modulation: a new technique in temperature-modulated DSC, Thermochim. Acta 446 (1–2) (2006) 147–155.
[93] A.P. Holt, et al., Controlling interfacial dynamics: covalent bonding versus physical adsorption in polymer nanocomposites, ACS Nano 10 (7) (2016) 6843–6852.
[94] S. Cheng, et al., Big effect of small nanoparticles: a shift in paradigm for polymer nanocomposites, ACS Nano 11 (1) (2017) 752–759.
[95] F. Barroso-Bujans, et al., Confinement of poly(ethylene oxide) in the nanometer-scale pores of resins and carbon nanoparticles, Soft Matter 9 (46) (2013) 10960–10965.
[96] F. Barroso-Bujans, et al., Macromolecular structure and vibrational dynamics of confined poly(ethylene oxide): from subnanometer 2D-intercalation into graphite oxide to surface adsorption onto graphene sheets, ACS Macro Lett. 1 (5) (2012) 550–554.
[97] K. Chen, C.A. Wilkie, S. Vyazovkin, Nanoconfinement revealed in degradation and relaxation studies of two structurally different polystyrene−clay systems, J. Phys. Chem. B 111 (44) (2007) 12685–12692.
[98] E. Zhuravlev, C. Schick, Fast scanning power compensated differential scanning nanocalorimeter: 1. The device, Thermochim. Acta 505 (1–2) (2010) 1–13.
[99] E. Zhuravlev, C. Schick, Fast scanning power compensated differential scanning nanocalorimeter: 2. Heat capacity analysis, Thermochim. Acta 505 (1–2) (2010) 14–21.
[100] C. Schick, Dynamic calorimetric glass transition in thin polymer films, in: F. Kremer (Ed.), Dynamics in Geometrical Confinement, Springer International Publishing, Cham, 2014, pp. 307–338.
[101] D.G. Papageorgiou, et al., Kinetics of nucleation and crystallization in poly(butylene succinate) nanocomposites, Polymer 55 (26) (2014) 6725–6734.
[102] T. Souier, et al., Nanoscale thermal analysis of multiphase polymer nanocomposites, J. Phys. Chem. C 116 (15) (2012) 8849–8856.
[103] A. Majumdar, J.P. Carrejo, J. Lai, Thermal imaging using the atomic force microscope, Appl. Phys. Lett. 62 (20) (1993) 2501–2503.
[104] B.A. Nelson, W.P. King, Measuring material softening with nanoscale spatial resolution using heated silicon probes, Rev. Sci. Instrum. 78 (2) (2007), 023702.
[105] M.P. Nikiforov, et al., Morphology mapping of phase-separated polymer films using nanothermal analysis, Macromolecules 43 (16) (2010) 6724–6730.
[106] S. Singh, C. Wu, P.T. Williams, Pyrolysis of waste materials using TGA-MS and TGA-FTIR as complementary characterisation techniques, J. Anal. Appl. Pyrolysis 94 (2012) 99–107.

[107] K. Pielichowski, J. Njuguna, L. Rapra Technology, Thermal Degradation of Polymeric Materials, Rapra Technology, Shawbury, 2005.
[108] A. Leszczyńska, et al., Polymer/montmorillonite nanocomposites with improved thermal properties: part II. Thermal stability of montmorillonite nanocomposites based on different polymeric matrixes, Thermochim. Acta 454 (1) (2007) 1–22.
[109] E. Roumeli, et al., Understanding the mechanical and thermal property reinforcement of crosslinked polyethylene by nanodiamonds and carbon nanotubes, RSC Adv. 4 (85) (2014) 45522–45534.
[110] E. Abraham, et al., Highly modified cellulose nanocrystals and formation of epoxy-nanocrystalline cellulose (CNC) nanocomposites, ACS Appl. Mater. Interfaces 8 (41) (2016) 28086–28095.
[111] H.W.P. Carvalho, et al., Polymer-clay nanocomposites thermal stability: experimental evidence of the radical trapping effect, RSC Adv. 3 (45) (2013) 22830–22833.
[112] F. Barroso-Bujans, et al., Thermal stability of polymers confined in graphite oxide, Macromolecules 46 (5) (2013) 1890–1898.
[113] K. Pielichowska, The influence of molecular weight on the properties of polyacetal/hydroxyapatite nanocomposites. Part 2. In vitro assessment, J. Polym. Res. 19 (2) (2012) 9788.
[114] K. Pielichowska, The influence of polyoxymethylene molar mass on the oxidative thermal degradation of its nanocomposites with hydroxyapatite, J. Therm. Anal. Calorim. 124 (2) (2016) 751–765.
[115] D.M. Price, D.J. Hourston, F. Dumont, Thermogravimetry of polymers, in: Encyclopedia of Analytical Chemistry, John Wiley & Sons, Ltd, Chichester, United Kingdom, 2006.
[116] M. Webb, P.M. Last, C. Breen, Synergic chemical analysis—the coupling of TG with FTIR, MS and GC-MS: 1. The determination of the gases released during the thermal oxidation of a printed circuit board, Thermochim. Acta 326 (1–2) (1999) 151–158.
[117] S. Materazzi, A. Gentili, R. Curini, Applications of evolved gas analysis: part 2: EGA by mass spectrometry, Talanta 69 (4) (2006) 781–794.
[118] S. Materazzi, A. Gentili, R. Curini, Applications of evolved gas analysis: part 1: EGA by infrared spectroscopy, Talanta 68 (3) (2006) 489–496.
[119] M. Kamruddin, et al., Thermogravimetry-evolved gas analysis-mass spectrometry system for materials research, Bull. Mater. Sci. 26 (4) (2003) 449–460.
[120] S. Materazzi, R. Curini, The coupling of mass spectrometry with thermoanalytical instruments: applications of evolved gas analysis, Appl. Spectrosc. Rev. 36 (2–3) (2001) 169–180.
[121] S. Materazzi, R. Curini, On-line evolved gas analysis by infrared spectroscopy coupled to thermoanalytical instruments, Appl. Spectrosc. Rev. 36 (1) (2001) 1–9.
[122] A.D. McNaught, A. Wilkinson, IUPAC Compendium of Chemical Terminology, second ed., Wiley-Blackwell, Oxford, UK, 1997.
[123] K. Pielichowska, Thermooxidative degradation of polyoxymethylene homo- and copolymer nanocomposites with hydroxyapatite: kinetic and thermoanalytical study, Thermochim. Acta (2015), https://doi.org/10.1016/j.tca.2014.11.016.
[124] Y.F. Duan, et al., Study on the thermal degradation of polyoxymethylene by thermogravimetry-fourier transform infrared spectroscopy (TG-FTIR), J. Appl. Polym. Sci. 99 (6) (2006) 3085–3092.
[125] J.M. Cervantes-Uc, et al., TGA/FTIR studies of segmented aliphatic polyurethanes and their nanocomposites prepared with commercial montmorillonites, Polym. Degrad. Stab. 94 (10) (2009) 1666–1677.

[126] W. Xie, et al., Thermal degradation chemistry of alkyl quaternary ammonium montmorillonite, Chem. Mater. 13 (9) (2001) 2979–2990.
[127] T. Takeichi, Y. Guo, Synthesis and characterization of poly(urethane-benzoxazine)/clay hybrid nanocomposites, J. Appl. Polym. Sci. 90 (14) (2003) 4075–4083.
[128] K. Chen, M.A. Susner, S. Vyazovkin, Effect of the brush structure on the degradation mechanism of polystyrene–clay nanocomposites, Macromol. Rapid Commun. 26 (9) (2005) 690–695.
[129] R. Zha, et al., Double dimensionally ordered nanostructures: toward a multifunctional reinforcing nanohybrid for epoxy resin, RSC Adv. 7 (2) (2017) 1177–1190.
[130] S.A. Pihan, et al., Soft nanocomposites—from interface control to interphase formation, ACS Appl. Mater. Interfaces 7 (23) (2015) 12380–12386.
[131] Z. Shi, et al., Three-dimensional nanoporous cellulose gels as a flexible reinforcement matrix for polymer nanocomposites, ACS Appl. Mater. Interfaces 7 (41) (2015) 22990–22998.
[132] X. Zhang, L.S. Loo, Study of glass transition and reinforcement mechanism in polymer/layered silicate nanocomposites, Macromolecules 42 (14) (2009) 5196–5207.
[133] J. Pagacz, et al., Bio-polyamides based on renewable raw materials, J. Therm. Anal. Calorim. 123 (2) (2016) 1225–1237.
[134] E.J. Donth, The Glass Transition: Relaxation Dynamics in Liquids and Disordered Materials, Physics and Astronomy Online LibrarySpringer, Heidelberg, 2001.
[135] K. Pielichowska, et al., The influence of nanohydroxyapatite on the thermal, mechanical and tribological properties of polyoxymethylene nanocomposites, Int. J. Polym. Sci. 9051914 (2017) 1–11.
[136] M. Wong, et al., Glass transition temperature changes of melt-blended polymer nanocomposites containing finely dispersed ZnO quantum dots, Soft Matter 6 (18) (2010) 4482–4490.
[137] P. Rittigstein, et al., Model polymer nanocomposites provide an understanding of confinement effects in real nanocomposites, Nat. Mater. 6 (4) (2007) 278–282.
[138] Y.-J. Kim, et al., Polyimide nanocomposites with functionalized SiO_2 nanoparticles: enhanced processability, thermal and mechanical properties, RSC Adv. 4 (82) (2014) 43371–43377.
[139] W.J. Parker, et al., Flash method of determining thermal diffusivity, heat capacity, and thermal conductivity, J. Appl. Phys. 32 (9) (1961) 1679–1684.
[140] P.S. Gaal, M.A. Thermitus, D.E. Stroe, Thermal conductivity measurements using the flash method, J. Therm. Anal. Calorim. 78 (1) (2004) 185–189.
[141] E.-Y. Choi, et al., Reinforcement of nylon 6,6/nylon 6,6 grafted nanodiamond composites by in situ reactive extrusion, Sci. Rep. 6 (2016) 37010.
[142] M. Abdalla, et al., Magnetically processed carbon nanotube/epoxy nanocomposites: morphology, thermal, and mechanical properties, Polymer 51 (7) (2010) 1614–1620.
[143] A. Vassilikou-Dova, I.M. Kalogeras, Dielectric analysis (DEA), in: Thermal Analysis of Polymers, John Wiley & Sons, Inc., Hoboken, NJ, 2009, pp. 497–613.
[144] A. Schönhals, F. Kremer, Theory of dielectric relaxation, in: F. Kremer, A. Schönhals (Eds.), Broadband Dielectric Spectroscopy, Springer Berlin Heidelberg, Berlin, Heidelberg, 2003, pp. 1–33.
[145] O.A. Al-Hartomy, et al., Properties of natural rubber-based composites containing fullerene, Int. J. Polym. Sci. 2012 (2012) 8.

[146] O.A. Al-Hartomy, et al., Dynamic mechanical thermal analysis and dielectric thermal analysis of siloxane rubber-based composites filled with carbon black, J. Compos. Mater. 46 (14) (2012) 1765–1770.
[147] Y. Rao, J.M. Pochan, Mechanics of polymer−clay nanocomposites, Macromolecules 40 (2) (2007) 290–296.
[148] V.V. Daniel, Dielectric Relaxation, Academic Press, New York, 1967.
[149] D.G. Bekas, et al., On the use of dielectric spectroscopy for the real time assessment of the dispersion of carbon nanotubes in epoxy, RSC Adv. 6 (82) (2016) 78838–78845.